Chaotic Motion Revealed by the Poincaré Section

By:

Harry Green

Project unit: PRO302
Supervisor: Dr. Thomas Waters

March 2012

Abstract

This dissertation examines the appearances of chaotic motion in dynamics, primarily using mechanics as a base for many of the systems used. Due to advances in the availability of computer technology, chaos theory is a popular area of modern mathematical research, allowing many forms of numerical analysis that were previously inaccessible. It is these methods that will be used to represent chaotic motion in the dissertation, by providing the computational power to plot Poincaré sections, among other types of plot. Poincaré sections build up a clear picture of how behaviour can change from regular to chaotic on different energy surfaces. The basis of the dissertation will use analytical mechanics, with heavy reliance on the Lagrangian and Hamiltonian functions, so the first sections of the dissertation will establish these, in detail. The system studied in the most detail will be the Hénon-Heiles Potential, and we will see both regular and chaotic motion by plotting Poincaré sections.

Acknowledgements

This dissertation would not have been possible without the excellent support and guidance of Dr. Thomas Waters throughout writing the project.

I'd also like to thank Nicola Pickering, for her thorough proof-reading of the dissertation, and the owners of http://www.scribtex.com for providing a very useful free online LaTeXcompiling service that I used to store and write the entire project.

The project would also have been significantly more difficult without access to the necessary computer software used for visualisation: MATLAB, Wolfram Mathematica, Adobe Photoshop, Macromedia Fireworks, Autodesk 3DS Max and Adobe Flash.

Contents

Chapter 1

Basic Introduction

The universe we live in is a constant state of change [2]. Dynamics is the science of change, and as such, has been a prominent research area in science since its creation. Chaos is an area of dynamics regarding the predictability of a dynamical system that attracted a great deal of interest in the second half of the 20th century. Before introducing chaos, it will be necessary to first give a brief introduction to dynamical systems in general. In short, dynamics is the study of a particle or object in motion. The field of dynamics has applications in very wide reaching fields, including physics, economics, and biology. In this dissertation, it will be more fitting to focus on classical mechanics as a background for real-world applications, for these are often the most descriptive scenarios. Classical mechanics, distinct from modern mechanics, deals with objects on a macroscopic scale, where the effects of general relativity and quantum physics are ignorable [2].

As the field of dynamics originally evolved from mechanics, there are a great deal of mechanical systems in the real world that display a wide range of behaviour in dynamics. It is this behaviour that we will explore in detail. Classical Mechanics is also a good background because, in theory at least, its systems are deterministic and easily predictable by solving the equations of motion by whatever method is appropriate.

This property links very well to the project, as the typical dynamical system is a deterministic set of differential equations that determine the movement of some point in phase space. The concept of phase space will be described later in the project. The dynamical system being defined as a set of differential equations leaves no room for randomness, that is to say

that a dynamical system is not in any way a stochastic process. However, under certain conditions, these regular, predictable, deterministic systems can produce unexpected and seemingly random behaviour. We will describe this behaviour as *chaotic*, and the purpose of this project is to analyse it in detail.

Introductions to chaos theory are never far from Edward Lorenz' so called 'Butterfly Effect', the metaphor that a butterfly's wing flap can alter the formation of a hurricane many weeks later. This is an interesting way of describing the mathematical phenomena of *sensitivity to initial conditions*.

A dynamical system is said to be sensitive to initial conditions if a very small change in initial conditions eventually results in a huge change in later behaviour. This is said to be a prerequisite for chaotic motion in dynamics. The other condition is that the system must be at least 3 dimensional. Chaotic motion typically generates graphs that are befitting of the adjective chaotic; however, there are often certain patterns amidst the apparent randomness. This is particularly seen in one of the most famous chaotic systems of the present day, the *Lorenz attractor* (Figure 1.1). The Lorenz attractor will not be explicitly used in the paper, but it displays many properties common with systems that will be seen in this project and serves as a good initial example.

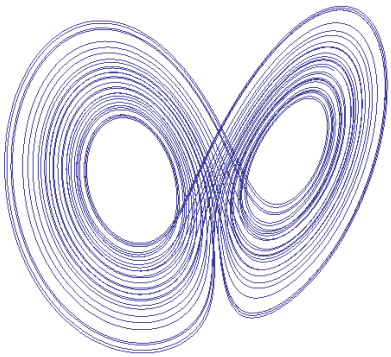

Figure 1.1: The *Lorenz Attractor*, plotted in Mathematica.

Chaos has taken a great leap in its level of attention in the last half a century thanks to the similar leaps of progression in the computer sciences. The two are extremely linked, because all studies of chaotic motion require

a great deal of computing power. This is why chaos was a largely unknown concept until recently. It is only with modern computers that we can see sensitivity to initial conditions by running repetitive iterations, differing the initial conditions by a seemingly insignificant value. These calculations require such precision that they were inaccessible to mathematicians in the era before the computer, although some, such as Henri Poincaré in the late 1800s, had visions of chaos that he lacked the tools to demonstrate. However, his work included the development of the Poincaré Section, a type of plot that was impossible to create at the time. We now have the computational power to perform the necessary calculations, and this will be the basis of many of our investigations into chaotic systems.

Other chaotic systems can arise from a much more mundane system. For continuous systems, provided the system displays at least 3 degrees of freedom, and is non-linear, it qualifies to be chaotic so long as there is a sensitivity to initial conditions. The double pendulum is an example of a system that is a simple concept, but results in extremely complicated behaviour that can be described as chaotic. While discrete systems are not the primary focus of this project, they can exhibit chaotic behaviour in a much simpler system, such as the one dimensional logistic map.

$$x_{n+1} \to 4x_n(1 - x_n) \tag{1.1}$$

which while apparently is a simple looking system, can display extreme sensitivity to initial conditions over a few iterations. While the dissertation will focus manly on continuous systems, it is worth noting the distinction between the two types of system, discrete and continuous. An example of a continuous chaotic dynamical system is the Lorenz Attractor. Chaotic systems like the Lorenz Attractor above appear in numerous areas of everyday life. Lorenz himself derived the attractor when trying to solve problems in weather forecasting [1]. The weather displays all the properties of a chaotic dynamical system. It is extremely sensitive to initial conditions, in that a very slight error in measurement would lead to a completely different prediction a few weeks later. This is represented in the Lorenz Attractor, in that very minor changes in initial conditions could lead to solutions that end up on completely different sides of the graph.

The exact equations that form the Lorenz Attractor are

$$\left.\begin{aligned} \dot{x} &= \sigma(y-x) \\ \dot{y} &= x(\rho-z)+y \\ \dot{z} &= xy-\beta z \end{aligned}\right\} \qquad \text{Lorenz' Equations [3]} \tag{1.2}$$

where a dot denotes differential with respect to t. For the plot in Figure (1.1), the values $\sigma = 10, \rho = 28, \beta = 8/3$ have been chosen. These are commonly used for plotting the Lorenz Attractor. This system is very similar to those that will be discussed later in the paper.

Chapter 2

Technical Introduction

Newton developed the concept of dynamics along with the creation of his laws of motion [2], laws that govern the motion of objects in classical mechanics. Newtonian mechanics generally involve heavy use of calculus and vector methods, with emphasis on the motion of an object caused by the forces acting on it. Solution of the resulting equations of motion gives a complete description of both the future and past motion of the object. While vector methods such as Newton's are sufficient to solve a wide range of problems, often for complicated systems the solution of the equations of motion becomes unnecessarily messy. For these systems, energy methods are more convenient and provide a neater solution.

As opposed to observing the forces acting on an object, analytical methods (also known as energy methods) derive the equations of motion using scalar quantities. These are typically broader in their applications than vector methods, and often allow for a simplification of the system by omitting ignorable co-ordinates that don't contribute to the changes in energy. While both vector and analytical methods will be used, often vector methods will simply serve as a starting point, and used to derive the total energy so that a continuation of the problem using analytical methods is possible. In this chapter we shall give definitions and proofs of the theory that will be required in the later chapters of the paper.

2.1 Generalised Coordinates and Momenta

Generalised Coordinates are what allow a complicated system in vector mechanics to be simplified in analytical methods. In contrast with the coordinate systems used in vector mechanics, analytical methods use generalised coordinates to define a system, which may or may not be a coordinate of physical space.

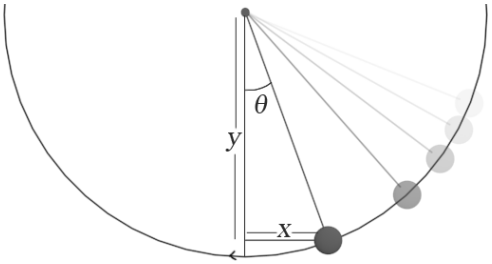

Figure 2.1: The idealised pendulum, a common example in classical mechanics. Rendered in Autodesk 3DS Max 2012

Fig. 2.1 shows a simple idealised pendulum. It is assumed to have no friction or air resistance, hanging on a string of length l that is light (assumed 0 mass) and inextensible. It is a good simple example of how analytical methods differ from vector methods. The pendulum is moving in the plane, and therefore can be described using two co-ordinates, x and y. Using this approach, at any point, the state of the system can be completely described by a vector $(x, y)^T$. Under analytic methods however, a simpler approach is used, by the realisation that only one coordinate is actually needed, the angle that the rod makes with the downward vertical.

The system, although it is described by a vector of two elements in vector methods, can be described in analytical methods simply by the value of the angle θ. Instead of using a two dimensional vector for each force to derive the equations of motion, using analytical methods only the scalar quantities of the *potential energy* and *kinetic energy* are required to solve the equations of motion. For general systems, generalised coordinates will be written as q_i, while x, y, and z (or in general x_i) shall continue to denote the physical coordinates.

Since x_i and q_i both uniquely specify the system, there must be a one to one relationship between the two, and the transformation must be invertible.

Specifically, for a one particle system in three dimensions,

$$x_i = x_i(q_1, q_2, q_3, t) \tag{2.1}$$

And since there must be an inverse,

$$q_i = q_i(x_1, x_2, x_3, t). \tag{2.2}$$

In the example of the pendulum, there is one less generalised coordinate than there are physical ones. Note that no information about the system is lost by the reduction of a coordinate, as the values of x and y can be obtained directly from θ in accordance with Equation (2.1):

$$x = l\cos\theta, \qquad y = l\sin\theta$$

.

Equation (2.2) is fulfilled by

$$\theta = \arctan\frac{x}{y}$$

Since the state of the system can be described in its entirety using only one coordinate, we say that the system has one *degree of freedom*. In general, a system has n degrees of freedom if a minimum of n coordinates are required to describe its state at any time. A system with n degrees of freedom typically has a $2n$ dimensional *phase space*. In this system, the dimensions of phase space are θ and $\dot{\theta}$.

In the above example, energy is conserved. For reasons that will become more clear later, we shall call such systems *Hamiltonian*, and temporarily define a *Hamiltonian System* as one in which the total energy is constant [8]. We can define an *integral* as a function of the coordinates of phase space which remains constant over time. If a system with n degrees of freedom also has n integrals, we call the system *integrable*. In all Hamiltonian systems, the total energy is an integral. Some more definitions are needed before we go onto deriving the Lagrangian and Hamiltonian.

Generalised velocities are defined as the rate of change of the generalised coordinates with respect to time.

$$\dot{q}_i = \frac{dq_i}{dt} \tag{2.3}$$

2.2 Energy and Forces

To establish the kinetic energy of a particle, we must briefly return to physical coordinates, since its form would change depending on the choice of generalised coordinates used. The total energy of the system is given by

$$T = \frac{1}{2}\sum_{i=i}^{N} m_i(\dot{x_i}^2 + \dot{y_i}^2 + \dot{z_i}^2), \tag{2.4}$$

which is commonly recognised from elementary physics. For our purposes however, using generalised coordinates, the equation for kinetic energy will be left as a general function of the generalised coordinates. We can then express the total energy as

$$T = T(\mathbf{q}, \dot{\mathbf{q}}, t) \tag{2.5}$$

where T is a function that can be found through the relationship between the generalised and spatial coordinates. The *generalised momentum* p for each generalised coordinate is then defined as

$$p_i = \frac{\partial T}{\partial \dot{q}_i} \tag{2.6}$$

For a conservative system, the potential energy V has no common form, but can always be expressed as some function of the generalised coordinates.

$$V = V(q_1 \dots q_n) \tag{2.7}$$

Since Equation (2.7) has no functional dependence on the generalised velocities $\dot{q}_i$, it follows that

$$\frac{\partial V}{\partial \dot{q}_i} = 0 \tag{2.8}$$

It is also important to establish the concept of a *force*, the catalyst for change in a Newtonian System. From Newton's Laws of Motion we have

$$F_x = m\ddot{x}, \tag{2.9}$$

which gives the force in one component direction. The total force F is simply the sum of all the component forces. Alternatively, we also have a

formula to establish the force directly from the potential energy function V, as long as the force has no explicit time dependence:

$$F_x = \frac{-\partial V}{\partial x} \tag{2.10}$$

Note the minus sign on the right hand side. This formula, through integration, also provides a more explicit form for V. In generalised coordinates, our definition of a *generalised force* is denoted as Q, and is given by

$$Q_k = \sum_{i=1}^{N} F_{xi} \frac{\partial x_i}{\partial q_k}. \tag{2.11}$$

In words, the above equation equates the generalised force Q_k in a coordinate direction with the sum of the forces in each spatial dimension multiplied by the partial derivative of that spatial dimension with respect to q_k. Like before, if the force has no explicit time dependence, we can express it in a different way:

$$Q_k = -\frac{\partial V}{\partial q_k}. \tag{2.12}$$

As the remainder of this chapter will make heavy use of partial and total derivatives, it will be worthwhile to take a short digression to establish these in more detail.

2.3 Partial and Total derivatives

The *partial derivative* is the derivative of a function with the other variables assumed to be constants [4]. For example, in the randomly selected function

$$f(x, y) = y^2 x^3 - \cos y, \tag{2.13}$$

the partial derivative with respect to the variable y is denoted with the ∂ signs, and is equal to

$$\frac{\partial f}{\partial x} = 3y^2 x^2 \tag{2.14}$$

This type of derivative ignores any dependencies that the variable y might have on x. To take these dependencies into account, we introduce the *total*

derivative, denoted with a standard d. In general, the total derivative of $f(x, y)$ with respect to x can be written as

$$\frac{df}{dx} = \frac{\partial f}{\partial x} + \frac{\partial f}{\partial y}\frac{dy}{dx} \tag{2.15}$$

If, for example, $y = \sin x$, The total derivative of the previous function with respect to x is then

$$\frac{df}{dx} = 3y^2x^2 + (2yx^3 + \sin y) \cdot \cos x \tag{2.16}$$

It is worthwhile to note that as a consequence of this, if the space variable x_i depends on n generalised coordinates, we can write the total derivative $\dot{x}$ as

$$\dot{x_i} = \frac{\partial x_i}{\partial t} + \sum_{j=1}^{n} \frac{\partial x_i}{\partial q_j}\dot{q_j} \tag{2.17}$$

2.4 Lagrange's Equations of Motion

As an alternative to Newton's Laws of Motion, this paper will primarily use *Lagrange's Equations of Motion*, as they are easier to use with generalised coordinates. This section will derive the equations of motion, and from it, the *Lagrangian Function*, which will be shown to be equal to $T - V$. The derivation will use an N particle system in 3 spatial dimensions, and is a slightly modified version of the one given by Török (page 108-113) [2].

First we recall from the previous chapters two useful definitions, and obtain $\dot{p}$ through taking the total derivative of Equation (2.6) with respect to t

$$\dot{p_k} = \frac{d}{dt}(p_k) = \frac{d}{dt}\left(\frac{\partial T}{\partial \dot{q_k}}\right) \tag{2.18}$$

$$T = \frac{1}{2}\sum_{i=1}^{N} m_i\left(\dot{x_i}^2 + \dot{y_i}^2 + \dot{z_i}^2\right) \tag{2.19}$$

Taking derivatives of Equation (2.19) with respect to $\dot{q}$ then gives

$$p_k = \frac{\partial T}{\partial \dot{q}_k} = \sum_{i=1}^{N} m_i \left(\dot{x}_i \frac{\partial \dot{x}_i}{\partial \dot{q}_k} + \dot{y}_i \frac{\partial \dot{y}_i}{\partial \dot{q}_k} + \dot{z}_i \frac{\partial \dot{z}_i}{\partial \dot{q}_k} \right) \tag{2.20}$$

Note that the half at the front of the sum is cancelled out by the coefficient created by differentiating the $\dot{x}_i^2$ term. Also, by differentiating Equation (2.17) partially with respect to $\dot{q}_k$, the first term is eliminated completely, and the the $\dot{q}$ is removed from the second term, leaving us with

$$\frac{\partial \dot{x}_i}{\partial \dot{q}_k} = \frac{\partial x_i}{\partial q_k} \tag{2.21}$$

Substituting Equation (2.21) back into Equation (2.20) allows us to express p_k as

$$\frac{\partial T}{\partial \dot{q}_k} = \sum_{i=1}^{N} m_i \left(\dot{x}_i \frac{\partial x_i}{\partial q_k} + \dot{y}_i \frac{\partial y_i}{\partial q_k} + \dot{z}_i \frac{\partial z_i}{\partial q_k} \right) \tag{2.22}$$

We now take the total time derivative of the Equation (2.22) using the product rule from elementary calculus. However, as the results will be extremely long, it will be worth working through the steps with only one variable, x, and then add the others in at the end, as they will follow the same procedure.

$$\frac{d}{dt} \left(m_i \dot{x}_i \frac{\partial x_i}{\partial q_k} \right) = m_i \ddot{x}_i \frac{\partial x_i}{\partial q_k} + m_i \dot{x}_i \frac{d}{dt} \frac{\partial x_i}{\partial q_k} \tag{2.23}$$

However, recall from Equation (2.9) the definition of a force. We can rewrite Equation (2.23) as

$$\frac{d}{dt} \left(m_i \dot{x}_i \frac{\partial x_i}{\partial q_k} \right) = F_{ix} \frac{\partial x_i}{\partial q_k} + m_i \dot{x}_i \frac{d}{dt} \frac{\partial x_i}{\partial q_k} \tag{2.24}$$

Now if we examine the far right of Equation (2.23), we obtain, from the theory discussed in Section (2.3),

$$\frac{d}{dt} \frac{\partial x_i}{\partial q_k} = \frac{\partial^2 x_i}{\partial t \partial q_k} + \sum_{j=1}^{n} \frac{\partial^2 x_i}{\partial q_j \partial q_k} \dot{q}_j \tag{2.25}$$

Now, by factoring out the partial derivative with respect to $\dot{q}_k$, we obtain, on the right hand side, the expression for $\dot{x}_i$ stated in Equation (2.17)

$$\frac{d}{dt}\frac{\partial x_i}{\partial q_k} = \frac{\partial}{\partial q_k}\left(\frac{\partial x_i}{\partial t} + \sum_{j=1}^{n}\frac{\partial x_i}{\partial q_j}\dot{q}_j\right)$$

$$\frac{d}{dt}\frac{\partial x_i}{\partial q_k} = \frac{\partial}{\partial q_k}\dot{x}_i$$

$$\frac{d}{dt}\frac{\partial x_i}{\partial q_k} = \frac{\partial \dot{x}_i}{\partial q_k}$$

When the total time derivative of Equation (2.22) is written out in full with y and z included, the two terms in this differential can be expressed as two separate summations, as follows:

$$\frac{d}{dt}\left(\frac{\partial T}{\partial \dot{q}_k}\right) = \underbrace{\sum_{i=1}^{N} m_i\left(F_{ix}\frac{\partial x_i}{\partial q_k} + F_{iy}\frac{\partial y_i}{\partial q_k} + F_{iz}\frac{\partial z_i}{\partial q_k}\right)}_{Q_k} + \underbrace{\sum_{i=1}^{N} m_i\left(\dot{x}_i\frac{\partial \dot{x}_i}{\partial q_k} + \dot{y}_i\frac{\partial \dot{y}_i}{\partial q_k} + \dot{z}_i\frac{\partial \dot{z}_i}{\partial q_k}\right)}_{\frac{\partial T}{\partial q_k}} \tag{2.26}$$

The first summation being equal to Q_k follows directly from the definition given in Equation (2.11). The second requires slightly more thought. We know that

$$\frac{\partial}{\partial q_k}\frac{1}{2}\dot{x}_i^2 = \dot{x}_i\frac{\partial \dot{x}_i}{\partial q_k} \tag{2.27}$$

Which allows us to rewrite the second summation in Equation (2.26) as

$$\frac{\partial}{\partial q_k}\left[\frac{1}{2}\sum_{i=1}^{N} m_i\left(\dot{x}_i^2 + \dot{y}_i^2 + \dot{z}_i^2\right)\right] \tag{2.28}$$

where the quantity in the square brackets is the definition of kinetic energy. Substituting all this back into Equation (2.26) and making trivial rearrangements:

$$\frac{d}{dt}\left(\frac{\partial T}{\partial \dot{q}_k}\right) - \frac{\partial T}{\partial q_k} = Q_k \tag{2.29}$$

Equation (2.29) is the general form of *Lagrange's Equations of Motion*. However, if we have a conservative system, Q_k takes the form of Equation (2.12), giving us

$$\frac{d}{dt}\left(\frac{\partial T}{\partial \dot{q}_k}\right) - \frac{\partial T}{\partial q_k} = -\frac{\partial V}{\partial q_k} \tag{2.30}$$

Also, in a *Lagrangian System*, the potential function V depends only on the generalised coordinates, and not the velocities, so

$$\frac{\partial V}{\partial \dot{q}} = 0 \tag{2.31}$$

meaning that we can add it or subtract it as we please. This allows us to rearrange Equation (2.29) into

$$\begin{aligned} \frac{d}{dt}\left[\frac{\partial (T-V)}{\partial \dot{q}_k}\right] - \frac{\partial (T-V)}{\partial q_k} &= 0 \\ \frac{d}{dt}\left(\frac{\partial \mathcal{L}}{\partial \dot{q}_k}\right) - \frac{\partial \mathcal{L}}{\partial q_k} &= 0 \end{aligned} \tag{2.32}$$

This is a very important equation, and will be referred to frequently throughout the project. The bracketed $T - V$ in particular is of importance. We will refer to this as the *Lagrangian Function*, or just the *Lagrangian*, denoted $\mathcal{L}$ as in the second version of Equation (2.32). Including functional dependence, we define the Lagrangian as

$$\mathcal{L}(\mathbf{q}, \dot{\mathbf{q}}, t) = T(\mathbf{q}, \dot{\mathbf{q}}, t) - V(\mathbf{q}). \tag{2.33}$$

2.5 The Hamiltonian Function

Now the Lagrangian Function and Lagrange's Equations of Motion have been established, next in line is the *Hamiltonian Function* and *Hamilton's Equations of Motion*, which are essentially a development on Lagrange's work. First it will be useful to note that Equation (2.6) - Equation (2.8) gives us

$$p_k = \frac{\partial \mathcal{L}}{\partial \dot{q}_k} \tag{2.34}$$

A comparison of Equations (2.30) and (2.18) allows us to re-express the first term of (2.30) as $\dot{p}_k$, and taking the second term over to the right hand side gives us

$$\dot{p}_k = \frac{\partial \mathcal{L}}{\partial q_k} \tag{2.35}$$

Equations (2.34) and (2.35) give us an alternative form of Lagrange's Equations of Motion that will be more useful when working with the Hamiltonian. For a conservative system, the Lagrangian has no dependence on t, and so we can express $\dot{q}_k$ as a function of q and p only. We then define the Hamiltonian Function, H, as

$$\begin{aligned} H &= \sum_{k=1}^{n} p_k \dot{q}_k - \mathcal{L} \\ H(q,p) &= \sum_{k=1}^{n} p_k \dot{q}_k(q,p) - \mathcal{L}(q, \dot{q}(q,p)) \end{aligned} \tag{2.36}$$

We can then redefine a *Hamiltonian System* as one in which the Hamiltonian is constant. The Hamiltonian Function has some very useful properties, that the remainder of this section will establish, using an adapted form of Török's proof on the Jacobi Energy Integral (page 123-124) to fit the definition of the Hamiltonian [2]. Firstly, the total time derivative of$\mathcal{L}$ with respect to t is

$$\frac{d\mathcal{L}}{dt} = \sum_{k=1}^{n} \frac{\partial \mathcal{L}}{\partial q_k} \dot{q}_k + \sum_{k=1}^{n} \frac{\partial \mathcal{L}}{\partial \dot{q}_k} \ddot{q}_k + \frac{\partial \mathcal{L}}{\partial t} \tag{2.37}$$

With a small rearrangement of Equation (2.32) we can rewrite this as

$$\frac{d\mathcal{L}}{dt} = \sum_{k=1}^{n} \frac{d}{dt}\left(\frac{\partial \mathcal{L}}{\partial \dot{q}_k}\right) \dot{q}_k + \sum_{k=1}^{n} \frac{\partial \mathcal{L}}{\partial \dot{q}_k} \ddot{q}_k + \frac{\partial \mathcal{L}}{\partial t} \tag{2.38}$$

and noting by use of the product rule that

$$\frac{d}{dt}\left(\dot{q}_k \frac{\partial \mathcal{L}}{\partial \dot{q}_k}\right) = \frac{d}{dt}\left(\frac{\partial \mathcal{L}}{\partial \dot{q}_k}\right) \dot{q}_k + \frac{\partial \mathcal{L}}{\partial \dot{q}_k} \ddot{q}_k$$

We can simplify Equation (2.38) into

$$\frac{d\mathcal{L}}{dt} = \frac{d}{dt}\left(\sum_{k=1}^{n} \dot{q}_k \frac{\partial \mathcal{L}}{\partial \dot{q}_k}\right) + \frac{\partial \mathcal{L}}{\partial t} \tag{2.39}$$

Moving the left hand side over and bringing it into the differential, and bringing the final term to the other side gives

$$\frac{d}{dt}\left(\sum_{k=1}^{n}\dot{q}_k\frac{\partial\mathcal{L}}{\partial\dot{q}_k}-\mathcal{L}\right)=-\frac{\partial\mathcal{L}}{\partial t} \tag{2.40}$$

From Equation (2.34), we can introduce p_k into the equation, and we are left with the definition of the Hamiltonian Function from Equation (2.36)

$$\begin{aligned}\frac{d}{dt}\left(\sum_{k=1}^{n}\dot{q}_k p_k-\mathcal{L}\right)&=-\frac{\partial\mathcal{L}}{\partial t}\\ \frac{dH}{dt}&=-\frac{\partial\mathcal{L}}{\partial t}\end{aligned} \tag{2.41}$$

This leaves us with an equation that equates the total differential of the Hamiltonian with respect to time with the partial differential of the Lagrangian. This means that for a system in which the Lagrangian does not explicitly depend on time (a conservative system), the Hamiltonian remains constant throughout the motion, and is an integral as defined in Section (2.1). We will now demonstrate that the Hamiltonian is equal to the total mechanical energy of the system, $T+V$.

If we observe that the $\dot{x}^2$ term in the kinetic energy formula is equal to Equation (2.17) squared, we can rewrite $\dot{x}^2$ as three separate terms, one of which is a homogenous quadratic in $\dot{q}$, one of which is linear, and the third is constant. The values of the coefficients are functions of the generalised coordinate, however for our purposes it doesn't matter exactly what the values are, so we will simply call them α, β and γ. The kinetic energy of the system can then be written as

$$T=\underbrace{\frac{1}{2}\sum_{j=1}^{3N}\sum_{k=1}^{3N}\alpha_{jk}\dot{q}_j\dot{q}_k}_{T_2}+\underbrace{\sum_{j=1}^{3N}\beta_j\dot{q}_j}_{T_1}+\underbrace{\gamma}_{T_0} \tag{2.42}$$

Where T_2 represents the terms quadratic in in the $\dot{q}_i$s, T_1 represents the linear terms, and T_0 represents the remaining terms. The Lagrangian can then be written as

$$\mathcal{L} = T_2 + T_1 + T_0 - V \tag{2.43}$$

Assuming that the potential energy function V depends only on generalised coordinates, and not on velocities or time, we have

$$\sum_{k=1}^{n} \dot{q}_k \frac{\partial \mathcal{L}}{\partial \dot{q}_k} = 2T_+T_1 \tag{2.44}$$

Subtracting the Lagrangian from Equation (2.44) would give the Hamiltonian. However, if we use the form of the Lagrangian from Equation (2.43), we obtain a much more convenient way to express the Hamiltonian:

$$H = T_2 - T_0 + V \tag{2.45}$$

However, if the change of coordinates does not depend explicitly on t (if a non-moving reference frame is used), the linear and quadratic terms become zero. For the purposes of this paper, we shall only pick generalised coordinates that do not depend on t, so we may always assume this condition. The Hamiltonian is then directly equal to the total energy of the system

$$H = T + V \tag{2.46}$$

now, from the analysis of Equation (2.41), we have the law of conservation of energy: the total energy of the system is equal to the Hamiltonian, which is constant for any unforced system. From now on, it will be more convenient to use $H = T + V$ when calculating the Hamiltonian.

Since T does not depend on q, we have

$$\frac{\partial H}{\partial q_k} = -\frac{\partial \mathcal{L}}{\partial q_k} \tag{2.47}$$

Using this and Equation (2.34) gives us

$$\dot{p}_k = -\frac{\partial H}{\partial q_k} \tag{2.48}$$

It can also be derived from the Lagrangian equations that

$$\dot{q}_k = -\frac{\partial H}{\partial p_k} \tag{2.49}$$

Equations (2.48) and (2.49) together are called *Hamilton's Equations of Motion*, and will be useful when deriving a theorem later in the project.

2.6 Fixed Points in a Dynamical System

In a dynamical system consisting of a set of differential equations, a fixed point is defined to be a point at which the velocity is equal to 0 in all directions. There are many different types of fixed point, which largely can be classified as stable or unstable. This is best illustrated by a series of examples from old lecture notes.

For the dynamical system

$$\dot{x} = x, \qquad \dot{y} = -y \tag{2.50}$$

the solutions for $x(t)$ and $y(t)$ can be found simply by usual methods of solving ordinary differential equations. The graph of $x(t)$ follows an exponential growth, and $y(t)$ behaves with exponential decay. By using arrows to illustrate first the growth and decay along the appropriate axes, and then filling in the gaps, we arrive at a graph called a *phase portrait* that shows the development of the dynamical system over time. This particular example creates a *hyperbolic fixed point* or *saddle point* which we will see in examples later.

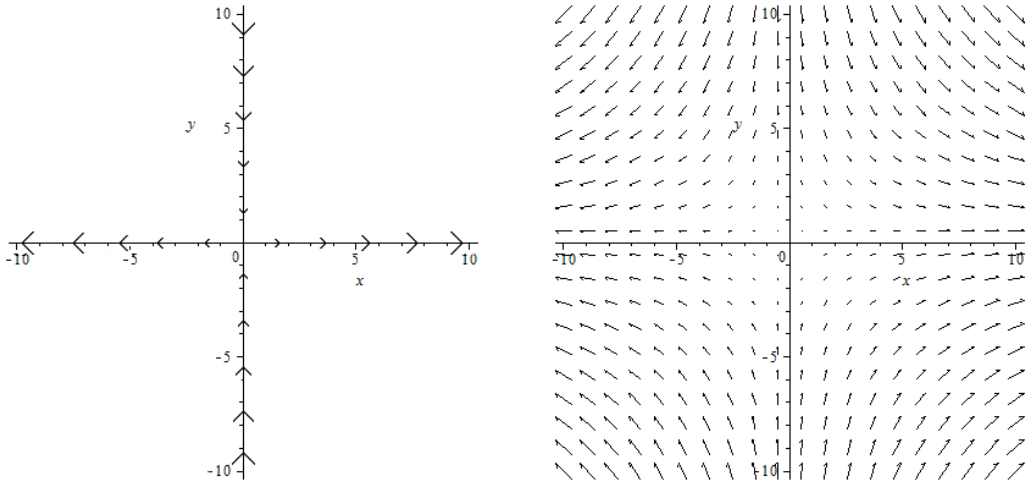

Figure 2.2: Creation of a saddle, with Maple and Photoshop

For the conservative systems that this project will describe, the only relevant types of fixed point are saddles (Figure 2.2), and centres, an illustration of which is shown below in Figure (2.3). The centre is generated by the dynamical system

$$\dot{x} = -y, \qquad \dot{y} = x \tag{2.51}$$

If we use the Jacobian Matrix to linearise the system about the fixed point, and find eigenvalues, we can determine the type of fixed point. Purely imaginary eigenvalues will result in a centre type fixed point, and real eigenvalues of opposite signs will create a saddle type. The alternative possibilities, such as two positive eigenvalues, will not arise from the conservative systems that this project will analyse.

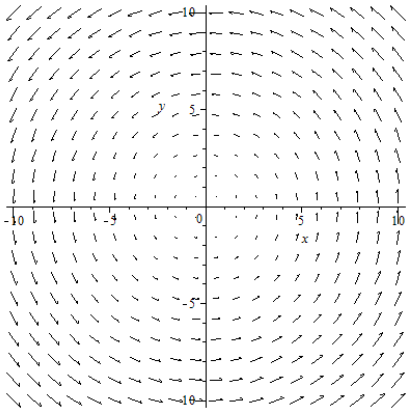

Figure 2.3: Creation of a centre, with Maple

The Jacobian Matrix of Equations (2.51) is found by differentiating each equation with respect to each variable. The result is the matrix $\mathcal{J}$.

$$\mathcal{J} = \begin{pmatrix} 0 & -1 \\ 1 & 0 \end{pmatrix} \tag{2.52}$$

We can then find the eigenvalues of this matrix by using the standard method, finding a characteristic equation by setting $\det(\lambda I - \mathcal{J}) = 0$. This results in the characteristic equation

$$\lambda^2 + 1 = 0. \tag{2.53}$$

Equation (2.53) trivially has solutions $\lambda = \pm i$, which is consistent with what was said earlier.

Chapter 3

Applications of Analytical Mechanics

3.1 Sliding Weights on a Frictionless Ramp

Now everything that we will need for energy methods is defined, we will use the Lagrangian to solve equations of motion analytically for a simple system with only one degree of freedom.

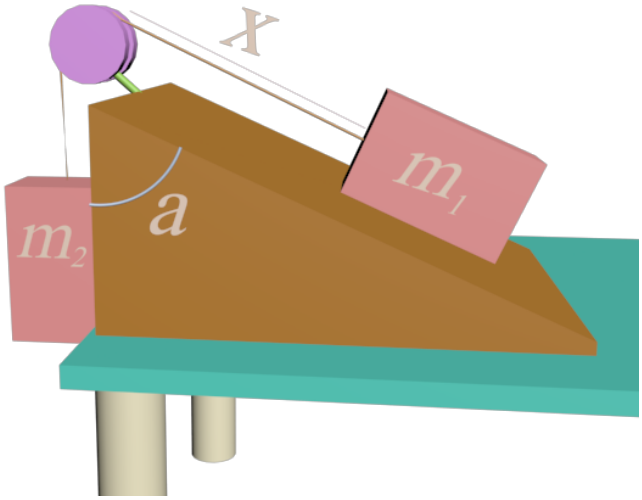

Figure 3.1: A pulley system with two masses

The following system is illustrated in Figure (3.1). It includes a ramp at angle θ and two masses, m_1 and m_2, connected by a light, inextensible string

of length l, which passes over a pulley. Both the ramp and pulley are assumed to be frictionless so that we have a conservative system. Although we have two particles move moving in a two dimensional system, we can simplify the amount of coordinates we need considerably by noting that both particles are moving along a straight line, and because the string is inextensible, by specifying the position of one mass we can calculate the other. For this reason, the only generalised coordinate we need, x, is the distance along the string between m_1 and the pulley. The distance between m_2 and the pulley is $l - x$.

The gravitational potential energy of m_1 can be found easily by

$$V_{m_1} = -m_1 g x \sin\theta \tag{3.1}$$

If we let the point of zero potential energy for m_2 be the lowest it can be $(x = 0)$, then an increase in x will raise m_2 by the same amount. We can then obtain a simple form of the potential energy of m_2:

$$V_{m_2} = m_2 g x \tag{3.2}$$

Equation (3.1) + Equation (3.2) gives the total potential energy of the system

$$V = m_2 g x - m_1 g x \sin\theta \tag{3.3}$$

As both masses travel at the same speed, the total kinetic energy of the system is simply

$$T = \frac{1}{2}\dot{x}^2(m_1 + m_2) \tag{3.4}$$

From Equations (3.3) and (3.4) we can find the Lagrangian to be

$$\mathcal{L} = \frac{1}{2}\dot{x}^2(m_1 + m_2) + gx(m_1 \sin\theta - m_2) \tag{3.5}$$

Now we can use Lagrange's Equations of Motion (Equation 2.32) to find an equation to describe the overall motion of the system. We will need to find the partial derivative of the Lagrangian with respect to x, then the time derivative of the partial derivative with respect to $\dot{x}$. This can all be performed with simple differentiation.

$$\frac{\partial \mathcal{L}}{\partial x} = g(m_1 \sin\theta - m_2) \tag{3.6}$$

$$\frac{\partial \mathcal{L}}{\partial \dot{x}} = \dot{x}(m_1 + m_2) \tag{3.7}$$

$$\frac{d}{dt}\frac{\partial \mathcal{L}}{\partial \dot{x}} = \ddot{x}(m_1 + m_2) \tag{3.8}$$

From this we can calculate the equation of motion for the system:

$$\ddot{x} = \frac{g(m_1 \sin\theta - m_2)}{m_1 + m_2} \tag{3.9}$$

For more complicated systems, these equations will be impossible (or at least extremely difficult) to solve analytically for the generalised coordinate, however, in this system, Lagrange's Equations of Motion have yielded a form that is easy to work with. Assuming that x has an initial velocity v_0 and initial position x_0, through integrating twice with respect to t we obtain

$$x = \frac{t^2}{2} \cdot \frac{g(m_1 \sin\theta - m_2)}{m_1 + m_2} + v_0 t + x_0 \tag{3.10}$$

3.2 Analysis of the Pendulum on a Moving Support

The previous example was useful for illustrating the practical applications of the technique, but was very simple. We will now use the same techniques for a more complicated system with more degrees of freedom. The example of an idealised pendulum on a moving support will be chosen to demonstrate the techniques. The system was recommended by my supervisor, but the analysis is my own.

The pendulum is an idealised pendulum, a bob of mass m and is assumed to swing only in the plane, on a light, inextensible string of length l with no friction. As opposed to Chapter (2.1) however, in this example, the pendulum's support (mass M) can move horizontally in the plane the pendulum is allowed to swing in. A diagram of this system is given in Figure (3.2). The support is assumed to be moving without friction, so that there are no

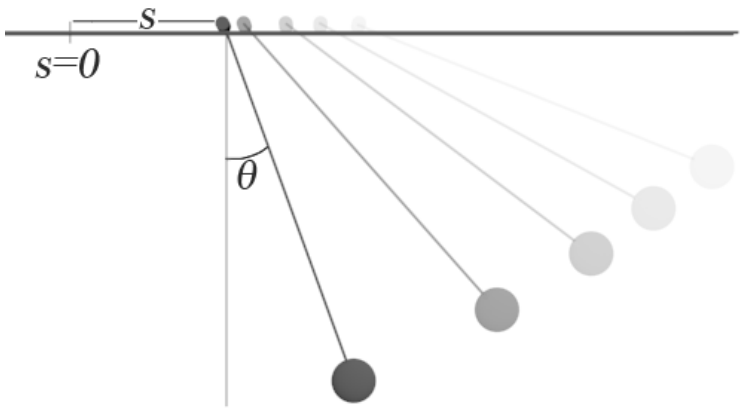

Figure 3.2: An illustration of a Pendulum on a Moving Support

external forces acting on the system. This means that the energy should remain constant throughout, and the system is Hamiltonian.

The system can be defined in terms of 2 generalised coordinates, s and θ, where s is the distance of the support from an arbitrary zero value and θ is the angle that the pendulum makes with the downward vertical.

If we assume the support level to be the zero level, the potential energy, V, is given by the displacement of the bob from the zero level multiplied by mg. Since the support is assumed to move horizontally on the zero level, the potential energy of the support itself is 0. Total potential energy is therefore:

$$V = -mgl\cos\theta. \tag{3.11}$$

To express the total kinetic energy T of the system in terms of generalised coordinates, we will need to temporarily refer back to vector methods. While the energy of the support T_M is simply given by

$$T_M = \frac{1}{2}M\dot{s}^2, \tag{3.12}$$

the kinetic energy of the bob is more complicated. The position of the bob in vector form can be expressed as

$$r = \begin{pmatrix} s + l\sin\theta \\ -l\cos\theta \end{pmatrix}.$$

Differentiating with respect to t,

$$\dot{r} = \begin{pmatrix} \dot{s} + l\dot{\theta}\cos\theta \\ l\dot{\theta}\sin\theta \end{pmatrix}.$$

Kinetic energy of the bob, T_m is then given by $\frac{1}{2}m||\dot{r}||$

$$T_m = \frac{1}{2}m((\dot{s} + l\dot{\theta}\cos\theta)^2 + (l\dot{\theta}\sin\theta)^2) \tag{3.13}$$

and finally, the total kinetic energy of the system T is equal to the sum of the two kinetic energies

$$T = \frac{1}{2}M\dot{s}^2 + \frac{1}{2}m((\dot{s} + l\dot{\theta}\cos\theta)^2 + (l\dot{\theta}\sin\theta)^2) \tag{3.14}$$

3.3 Applying the Lagrangian to the Moving Pendulum

Now we have the total potential energy (Equation 3.11) and the total kinetic energy (Equation 3.14), we can calculate the Lagrangian as $\mathcal{L} = T - V$

$$\begin{aligned} \mathcal{L} =& \frac{1}{2}M\dot{s}^2 + \frac{1}{2}m\left((\dot{s} + l\dot{\theta}\cos\theta)^2 + (l\dot{\theta}\sin\theta)^2\right) + mgl\cos\theta \\ =& \underbrace{\frac{1}{2}(M+m)\dot{s}^2 + ml\dot{\theta}\dot{s}\cos\theta + \frac{1}{2}ml^2\dot{\theta}^2}_{T} + \underbrace{mgl\cos\theta}_{-V} \end{aligned} \tag{3.15}$$

Now that we have the Lagrangian in terms of the generalised coordinates, we can use Equation (2.23) for each coordinate to determine the equations of motion in the form of a pair of differential equations.

Firstly, for the support coordinate s:

$$\frac{d}{dt}\left(\frac{\partial\mathcal{L}}{\partial\dot{s}}\right) - \frac{\partial\mathcal{L}}{\partial s} = 0$$

Using standard differentiation rules, we can calculate $\frac{\partial\mathcal{L}}{\partial s}$ and $\frac{\partial\mathcal{L}}{\partial\dot{s}}$. Since s does not appear at all in $\mathcal{L}$, $\frac{\partial\mathcal{L}}{\partial s} = 0$. Therefore, from equation (2.32),

$$\frac{d}{dt}\left(\frac{\partial \mathcal{L}}{\partial \dot{s}}\right) = 0$$

$$\frac{d}{dt}((M+m)\dot{s} + ml\dot{\theta}\cos\theta) = 0 \tag{3.16}$$

Equation (3.16) provides us almost directly with one of the equations of motion of the system. By evaluating the differential with respect to t, we obtain the result

$$(M+m)\ddot{s} + ml\ddot{\theta}\cos\theta - ml\dot{\theta}^2\sin\theta = 0, \tag{3.17}$$

which is one of the equations of motion with which we can completely describe the system's behaviour. The other is found by performing the same procedure for the other coordinate, θ.

$$\frac{d}{dt}\left(m(l\dot{s}\cos\theta + l^2\dot{\theta})\right) + m(l\dot{s}\dot{\theta} + gl)\sin\theta = 0$$

$$\ddot{\theta} + \frac{\dot{x}}{l}\cos\theta + \frac{g}{l}\sin\theta = 0 \tag{3.18}$$

Equations (3.17) and (3.18) provide us the means to (theoretically at least) predict the future or determine the past behaviour of the system for any length of time. The actual solution of the equations analytically is beyond the scope of this project, and their solution via numerical analysis, while not a difficult task, would be too much of a diversion. Equations of this type will be analysed in more detail later in the project using the Poincaré Section to locate chaotic behaviour in the solutions. For now, it is sufficient to know that the equations of motion exist in the form of a set of differential equations, and can be found with relative ease using the Lagrangian function.

3.4 The Hamiltonian of the Moving Pendulum

Now the Lagrangian for the system and equations of motion have been found, we can use the moving pendulum example to illustrate some properties of the Hamiltonian Function in a physical example. We will revert to the original

definition of the Hamiltonian given in Equation (2.36) for the time being. First we will need to find the generalised momenta, p_θ and p_s, of the system.

$$p_s = \frac{\partial \mathcal{L}}{\partial \dot{s}} = (M+m)\dot{s} + ml\theta\cos\theta \tag{3.19}$$

$$p_\theta = \frac{\partial \mathcal{L}}{\partial \dot{\theta}} = ml\dot{s}\cos\theta + ml^2\dot{\theta} \tag{3.20}$$

From this, and the Lagrangian from Equation (3.15), we can calculate the Hamiltonian Function for the moving pendulum:

$$\begin{aligned} H =& \dot{\theta}\left(ml\dot{s}\cos\theta + ml^2\dot{\theta}\right) + \dot{s}\left((M+m)\dot{s} + ml\theta\cos\theta\right) \\ & - \left(\frac{1}{2}(M+m)\dot{s}^2 + ml\dot{\theta}\dot{s}\cos\theta + \frac{1}{2}ml^2\dot{\theta}^2 + mgl\cos\theta\right) \\ H =& \frac{1}{2}(M+m)\dot{s}^2 + ml\dot{\theta}\dot{s}\cos\theta + \frac{1}{2}ml^2\dot{\theta}^2 - mgl\cos\theta \end{aligned} \tag{3.21}$$

By comparing this with the forms of T and V given in Equation (3.15), we can see what we showed before in the technical introduction, that the Hamiltonian is precisely equal to the potential energy of the system, $T+V$. We will now show that the Hamiltonian (and hence, the total energy) of the system is a constant at all times by differentiating with respect to t. After some lengthy calculations using standard differentiation procedures, we arrive at

$$\frac{dH}{dt} = (M+m)\dot{s}\ddot{s} + m\ddot{s}l\dot{\theta}\cos\theta + m\dot{x}l\ddot{\theta}\cos\theta - m\dot{x}l\dot{\theta}^2\sin\theta + ml^2\dot{\theta}\ddot{\theta} + mgl\sin\theta\dot{\theta} \tag{3.22}$$

While this is not a very helpful or descriptive format, with some factoring and rearrangement, Equation (3.22) can be rewritten as:

$$\frac{dH}{dt} = \dot{s}\left((M+m)\ddot{s} + ml\ddot{\theta}\cos\theta - ml\dot{\theta}^2\sin\theta\right) + l^2\dot{\theta}m\left(\ddot{\theta} + \frac{\dot{x}}{l}\cos\theta + \frac{g}{l}\sin\theta\right) \tag{3.23}$$

where the quantities in brackets are equal to the left hand sides of Equations (3.17) and (3.18), which we already established were equal to zero. Therefore, the total time derivative of H is 0, and H is a constant for all time.

3.5 Integrability and Tori

From Equation (3.15), which gave us the Lagrangian, we can analyse the *integrability* of the system. The Lagrangian depends only on θ, $\dot{\theta}$, and $\dot{s}$, so the derivative with of the Lagrangian with respect to s is equal to zero. We can call s an *ignorable coordinate*, as the Lagrangian doesn't depend on it. This gives us

$$\frac{d}{dt}\left(\frac{\partial \mathcal{L}}{\partial \dot{s}}\right) = 0 \tag{3.24}$$

Equation (3.24) has implications with regards to integrability not discussed earlier. The total time derivative of a function being equal to zero shows that the function is constant for all time. This fits the definition of an integral as discussed in Chapter (2.1), and so $\frac{\partial \mathcal{L}}{\partial \dot{s}}$ is an integral of the system. This, combined with the total energy being constant, gives us two integrals, and as the system also has two degrees of freedom, we can say that the pendulum on a moving support is integrable.

It is a consequence of the *Liouville-Arnold Theorem* [6] (proof of which is beyond the scope of this project), that if a system is integrable, its trajectories will lie on a torus. This applies to all integrable systems and to some non-integrable ones at certain energy levels, as will be seen in an analysis of the Hénon - Heiles system in Chapter 4. If trajectories on the tori remain on the tori, they are called *invariant tori*.

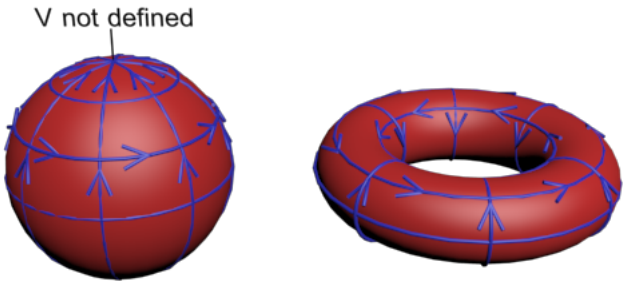

Figure 3.3: A model showing the topological differences between vector fields on the sphere and the torus.

For bounded motion, the system can only occupy a finite region of phase space, which can be represented as a curve on some manifold M. Motion on the manifold must be smooth and continuously differentiable. If we define V as a vector field on the torus describing the rate of change the coordinates, it can be plotted on the torus without singularity, unlike in the case of the sphere (Figure 3.3). In general, for an N dimensional system, the trajectories will lie on an $N + 1$ dimensional manifold called an N-torus.

If a trajectory starting on the torus stays on the torus, we can call it an *invariant torus*. For regular motion, which is typically periodic or quasi-periodic, trajectories can be easily represented on the torus. However, for chaotic motion, the tori are destroyed, which shall be seen later in the project.

Chapter 4

The Hénon and Heiles System

4.1 Background of the System

We will now perform a rather lengthy analysis of a specific system; one that can result in *chaotic motion* under certain energy levels, and can be analysed using the analytical mechanics described in the previous chapters. Rather than being taken directly from any physical system, in a paper studying integrals of motion in 1963, Michel Hénon and Carl Heiles chose a potential function purely for its mathematical properties. Desiring an equation that was both 'analytically simple', and 'sufficiently complicated to give non-trivial solutions' [9]. The potential chosen was a polynomial in x and y,

$$V = \frac{1}{2}\left(x^2 + y^2 + 2x^2y - \frac{2}{3}y^3\right) \tag{4.1}$$

4.2 Lagrangian Analysis

While the potential came directly from Hénon and Heiles' work, the analysis is my own. Our first step will be to use Lagrange's Equations of Motion to find equations to describe the system's behaviour. The system has two degrees of freedom, with the generalised coordinates simply being the Cartesian coordinates x and y. This results in a trivial evaluation of the kinetic energy:

$$T = \frac{1}{2}\left(\dot{x}^2 + \dot{y}^2\right) \tag{4.2}$$

From Equations (4.1) and (4.2), we can calculate the Lagrangian:

$$\mathcal{L} = \frac{1}{2}\left(\dot{x}^2 + \dot{y}^2\right) - \frac{1}{2}\left(x^2 + y^2 + 2x^2y - \frac{2}{3}y^3\right) \tag{4.3}$$

Now, as before, Lagrange's Equations of Motion will allow us to describe the system. First we find the derivatives of the Lagrangian with respect to the coordinates and velocities:

$$\frac{d}{dt}\frac{\partial \mathcal{L}}{\partial \dot{x}} = \ddot{x}$$
$$\frac{d}{dt}\frac{\partial \mathcal{L}}{\partial \dot{y}} = \ddot{y}$$
$$\frac{\partial \mathcal{L}}{\partial x} = -x - 2xy$$
$$\frac{\partial \mathcal{L}}{\partial x} = -y - x^2 + y^2$$

This allows us to simply write down the equations of motion for the system:

$$\ddot{x} = -x - 2xy \tag{4.4}$$

$$\ddot{y} = -y - x^2 + y^2 \tag{4.5}$$

From Equations (4.4) and (4.5) we can plot trajectories to track the motion of the system through time, allowing us to predict the future or determine the past given a set of initial conditions (x,y,$\dot{x}$,$\dot{y}$). Due to the four degrees of freedom in this system, the phase portrait becomes four dimensional, and requires special plotting techniques. For now though, we shall plot trajectories in the (x-y) plane. Finding an analytic expression in the form $x = x(t)$, $y = y(t)$ is too difficult (if it's even possible) and numerical approximations are the most appropriate way to proceed. The following analysis will be performed using the numerical integration functions of Wolfram Mathematica.

Each set of initial conditions will lead to a certain value for the Hamiltonian, which as established before is equal to the total mechanical energy of the system, and is constant. The changes in the energy level will cause changes in the behaviour of the system, ranging from simple to chaotic, as will be shown in the following section.

4.3 Bounded and Unbounded Motion

As the Hénon and Heiles system works in Cartesian coordinates, it is, in theory, possible for the system to escape to infinity if it has a high enough energy level. If the coordinates (x, y) of the system tend to infinity, we call this *unbounded motion*, and conversely, if (x, y) remain within some finite region, we call this *bounded motion*.

We can be more definite about this distinction by plotting the equipotential lines of the potential function V. When the potential function intersects the *energy surface*, $H = V$, and therefore $T = 0$, and the system has lost all of its kinetic energy. Therefore the coordinates (x, y) of trajectories on the energy surface $H = E$ are bounded by the equipotential lines $V = E$.

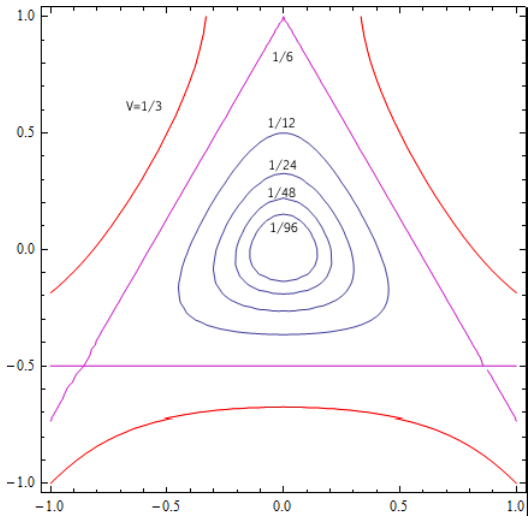

Figure 4.1: Equipotential lines of Equation (4.1)

The equipotential lines for various level sets of the Hénon and Heiles potential are shown in Figure (4.1). We can see from this that at energy levels greater than 1/6 the motion is unbounded, represented by the red lines not enclosing a simple region. At energy precisely equal to 1/6, the system is bounded by an equilateral triangle (as long as it starts in the triangle, otherwise it is unbounded). The equipotential lines become more circular at lower energy levels. Because we will only analyse bounded motion in this project, for the Hénon and Heiles' system a 'high energy level' is taken to be

one that approaches 1/6, and we will call 1/6 the *disassociation energy*.

Figure (4.1) was plotted using the following Mathematica loop to give an appropriate range of energy levels. The labelling and colouring was done in a graphics program, Macromedia Fireworks MX 2004.

```
U = 1/2 (x^2 + y^2 + 2 x^2*y - 2/3 y^3)
plots = Range[6];
For[i = 1;, i < 7, i++,
plots[[i]] =
ContourPlot[U == 1/(3*2^(i - 1)), {x, -1, 1}, {y, -1, 1}]]
Show[plots]
```

4.4 Regular Motion at low Energy Levels

First we will pick a set of initial conditions with a low energy level, which will give regular motion. The initial conditions were chosen to be $(x, y, \dot{x}, \dot{y})(0) = (0, 0.2, 0.2, 0.1)$. Calculating the Hamiltonian as $H = T + V$, we know that

$$H = \frac{1}{2}\left(\dot{x}^2 + \dot{y}^2\right) + \frac{1}{2}\left(x^2 + y^2 + 2x^2y - \frac{2}{3}y^3\right) \tag{4.6}$$

and from this it follows that the energy level of the system for the given initial values is $0.042\dot{3}$. This value will be relevant when we compare the results to different energy levels. As the energy depends on the four degrees of freedom, the condition for energy being a constant value can be expressed as $f(x, y, \dot{x}, \dot{y}) = C$, which is equivalent to defining a level set on a 4-dimensional surface. For this reason, we can say that the set of all points $f(x, y, \dot{x}, \dot{y}) = C$ lie on the same energy surface.

The simplest way to describe the behaviour of the system is to plot a trajectory in the (x-y) plane, which will be done numerically using Wolfram Mathematica. Firstly, the initial conditions above, and the equations of motion given in Equations (3.4) and (3.5), were defined as variables in Mathematica, then the following commands were used to plot a trajectory, using t as a parameter that ranges between 0 and 400:

```
sol = NDSolve[{eqn1 == 0, eqn2 == 0, x[0] == ics[[1]],
y[0] == ics[[2]], x'[0] == ics[[3]], y'[0] == ics[[4]]},
```

```
{x, y}, {t, 0, 400}];
ParametricPlot[Evaluate[{x[t], y[t]} /. sol], {t, 0, 400}]
```

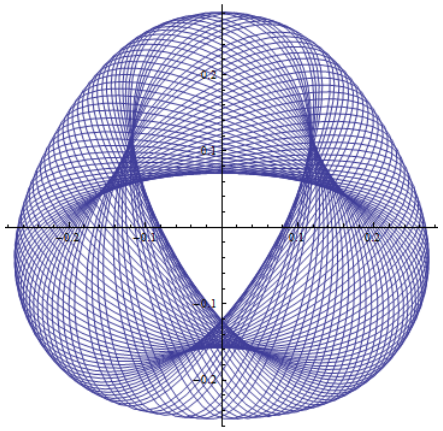

Figure 4.2: This is a trajectory on the energy surface $0.042\dot{3}$

The results are displayed in Figure (4.2). The behaviour of the system under this energy level, although complicated, is regular and follows a clear pattern. The specific value of $0.042\dot{3}$ for the energy isn't anything special, any energy level nearby will lead to similar results, this merely serves an example of the general case. The regularity of the motion means that two initial conditions close together on that energy surface will remain close together for all time. In other words, this energy level has very little sensitivity to initial conditions.

We can see this visually by taking two points close together on the same energy surface, and plotting how one coordinate (for example x) changes with time. Reducing the graph to one coordinate when comparing two trajectories gives us a clearer of how they diverge from each other as time changes. The technical procedure for this is to vary the value for one initial condition, for example x, very slightly, increasing to from x to $x + \delta$ where δ is very small, keep $\dot{x}$ and $\dot{y}$ at as they were before, then find the value of y that keeps the trajectory on the same energy surface. The value of $\delta = 0.001$ will be chosen for the purpose of this analysis.

Applying this perturbation to the initial conditions used previously gives $(x, y, \dot{x}, \dot{y})(0) = (0.001, y_0, 0.2, 0.1)$, where the value of y_0 remains to be

solved, although it seems reasonable that it would be close to the previous value of 0.2. As the final result will be a graph plotted in Mathematica, it makes more sense to use Mathematica to solve for y_0 rather than solving it by hand. The following Mathematica code was written for this purpose:

```
H = 1/2 (xdot^2 + ydot^2) + 1/2 (x^2 + y^2 + 2*x^2*y - 2/3 y^3)
Hy= Solve[{H /. {x ->0.001, xdot ->0.2, ydot ->0.1}} == 127/3000, y]
```

This gives the output of

```
{{y -> -0.176134}, {y -> 0.199996}, {y -> 1.47614}}
```

From which it is clear that the value we want is $y = 0.199996$, the other solutions are merely a result of a cubic having 3 roots and are unimportant to us now. The sets of initial conditions were then compared by plotting x against t, as shown below.

```
Plot1 = Plot[Evaluate[{x[t]} /. sol], {t, 0, 400}]
sol2 = NDSolve[{eqn1 == 0, eqn2 == 0, x[0] == ics2[[1]],
    y[0] == ics2[[2]], x'[0] == ics2[[3]], y'[0] == ics2[[4]]}, {x,
    y}, {t, 0, tend}];
Plot2 = Plot[Evaluate[{x[t]} /. sol2], {t, 0, 400}, PlotStyle -> Red]
Show[Plot1, Plot2]
```

The Mathematica commands were written to plot both sets of initial conditions individually, then display them both on the same axes.

Figure (4.3) shows the results of this analysis. Under small perturbations, there was barely any change in the system's behaviour over a long period of time, which can be seen by the similarities between Figures (4.3)(a) and (4.3)(b), and when they are plotted on one set of axes (Figure 4.3 c), they look like one line. It may seem obvious that initial conditions originally so close together would produce solutions that remain close together, but as we shall see shortly, this is not always the case for higher energy levels.

4.5 Chaotic Motion in the Hénon and Heiles system

For trajectories on energy surfaces corresponding to higher energy levels, the regularity of the behaviour begins to break down as it gains complexity.

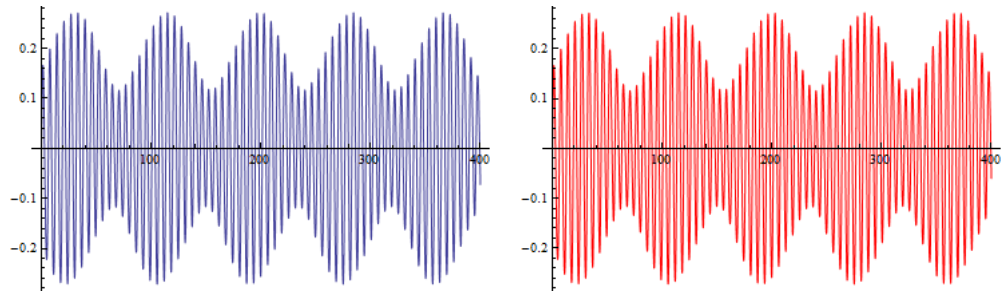

(a) Plot of x for original initial conditions (b) Plot of x for perturbed initial conditions

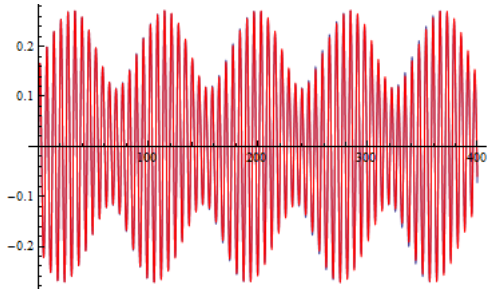

(c) Both lines plotted on the same axes

Figure 4.3: The plots generated by the above code

The methods of analysing this will be essentially the same methods used previously, but with increasingly higher energy levels, and we will see that the trajectories gain complexity before losing regularity and becoming fully chaotic, with extreme sensitivity to initial conditions.

As the equation for the Hamiltonian features largely positive polynomial terms, we can easily control the level of energy by raising and lowering the initial conditions. If we raise them slightly, to $(x, y, \dot{x}, \dot{y})(0) = (0, 0.2, 0.3, 0.2)$, the energy level becomes $0.082\dot{3}$. Plotting the trajectories in the same way as Figure (4.2), the pattern of the trajectory becomes more complicated, but still sticks to a regular pattern. The plot for a normal trajectory on this energy surface is seen in Figure (4.4).

When we raise the energy level even further, all pattern in the trajectory gives way to chaotic motion. In their paper, Hénon and Heiles showed that if the energy level becomes greater than $1/6$ [9], the energy becomes unbounded, so as we raise the energy level, we seek to stay below this value. The initial conditions $(x, y, \dot{x}, \dot{y})(0) = (0, 0.3, 0.4, 0.2)$ lie on the energy sur-

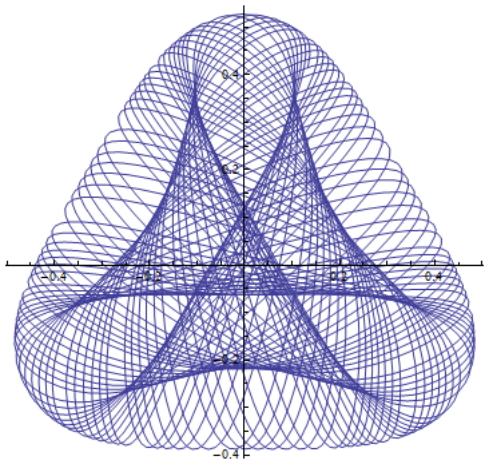

Figure 4.4: This is a trajectory on the energy surface $H = 0.082\dot{3}$

face $H = 0.161$, which is beginning to approach the boundary found by Hénon and Heiles. At this level, chaotic motion is easy to see in the parametric plot of Figure (4.5):

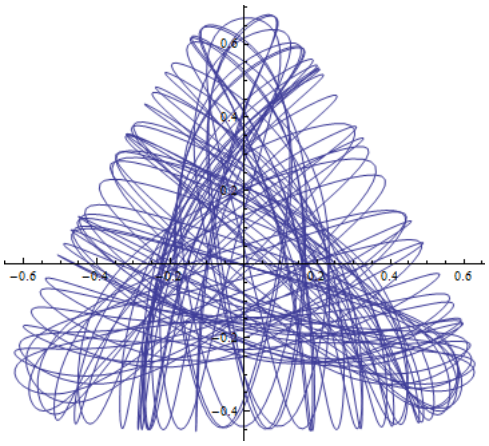

Figure 4.5: Energy surface 0.161, chaotic motion is seen

While it is clear now from Figure (4.5) that the system loses regularity at high energy levels, it remains to be seen that the system develops a high sensitivity to initial conditions. Through experimentation, we can raise the initial conditions in such a way to maximise the energy without losing boundedness. Solving for $H = 1/6$ isn't an option due to the numerical integration

error in Mathematica's approximation: the energy level changes very slightly due to this error, and if we start on the energy surface exactly equal to 1/6, it would quickly become unbounded. Experimentation gives the initial conditions $(x, y, \dot{x}, \dot{y})(0) = (0.08, 0.31, 0.4, 0.3)$ as a good set of initial conditions, giving the energy value at $H = 0.168034$. Ideally, this energy surface should contain trajectories with high sensitivity to initial conditions.

To test this, we will perform the same procedure as in Section 4.3, by slightly modifying the initial value of x to $x + \delta$. Experimentation suggests that $\delta = 0.0001$ gives a more descriptive picture than the previous value of $\delta = 0.001$. This should keep the trajectories closer together than if δ was 0.001. In order to keep the trajectories on the same energy surface, we must then solve for one of the other initial conditions. Using Mathematica to solve $H(0.0801, y, 0.4, 0.3) = 0.168034$ gives $y = 0.30973$. Therefore the sets of initial conditions that we need to compare are $(x, y, \dot{x}, \dot{y})(0) = (0.08, 0.31, 0.4, 0.3)$ and $(x, y, \dot{x}, \dot{y})(0) = (0.0801, 0.30973, 0.4, 0.3)$.

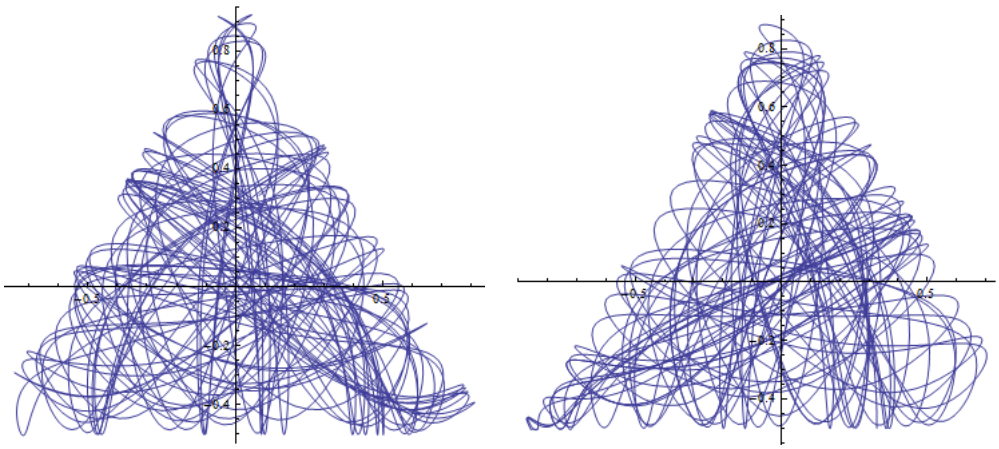

(a) Trajectory starting on $(x, y, \dot{x}, \dot{y})(0) = (0.08, 0.31, 0.4, 0.3)$

(b) Perturbed trajectory starting on $(x, y, \dot{x}, \dot{y})(0) = (0.0801, 0.30973, 0.4, 0.3)$

Figure 4.6: Trajectories with similar initial conditions side by side

It is easy to see simply by observation of Figure (4.6) that the two trajectories are massively different despite only a tiny change in the initial conditions. However, while it is clear to see that they are different, the nature of bounded chaotic motion turns both trajectories into a triangular shaped mess, and any form of comparison beyond simply stating 'they are different'

is impossible. For this, we use the same kind of graph seen in Figure (4.3 c), which can show us how the trajectories diverge from each other over time. This representation, seen in Figure (4.7), gives us a much clearer picture.

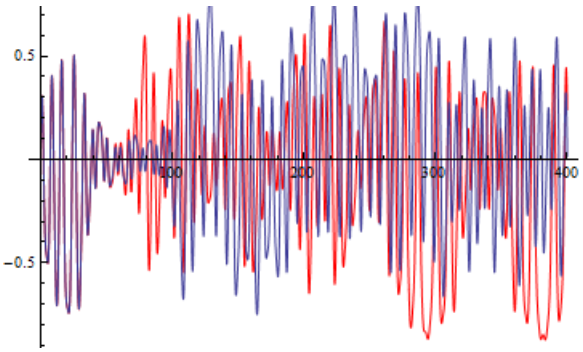

Figure 4.7: Plot of $x(t)$ for both sets of initial conditions

We can see that initially, the two graphs follow the same path, corresponding to their near-identical initial conditions. By about $t = 50$, the graphs begin to visibly diverge from each other, and at $t = 75$ they don't resemble each other at all, the amplitude in the perturbed system much larger than that of the original system. From then on, there is no similarity between the two graphs, and there is no indication that they started so close together at $t = 0$. This is an example of a Sensitivity to Initial Conditions, a feature of chaotic systems, where a small change in initial conditions leads to a large change in the result.

This contrasts greatly with the results seen on the regular energy surfaces of Figure (4.2), where small perturbations barely caused any noticeable change in the system. Although the value ofδ changed between the two energy surfaces, this was only to keep the trajectories on the higher energy surface *closer* together. Using $\delta = 0.001$ for both caused them to diverge far too quickly to make Figure (4.7) descriptive. This is an example of how a system can behave regularly at small energy levels, and become chaotic as the energy increases.

4.6 Meromorphically Integrable Systems

In the example of the moving pendulum example we found an ignorable coordinate s, and this provided us with an integral. With the Hamiltonian, this gave us two integrals, and so we could say that the system is integrable. In the Hénon and Heiles system though, we have no ignorable coordinates, and so it is unclear whether or not the system is integrable. This can be done by an analysis of polynomial potentials in general.

A polynomial potential function is simply the sum of powers of q (x and y in the case of Hénon and Heiles). A potential $V(\mathbf{q})$ can then be written in terms of increasing order as

$$V(\mathbf{q}) = V_{\min}(\mathbf{q}) + \cdots + V_{\max}(\mathbf{q})$$

where min and max represent the lowest and highest order terms. As an example, x^2y is taken to be of order 3. The individual terms can then be split up and represented as their own Hamiltonian systems [11], by adding the kinetic energy, as follows:

$$H_{\min} = \frac{1}{2}\sum_{i=t}^{n} p_i^2 + V_{\min}(\mathbf{q}) \qquad H_{\max} = \frac{1}{2}\sum_{i=i}^{n} p_i^2 + V_{\max}(\mathbf{q})$$

For a system with 2 degrees of freedom x and y, $V(x, y)$ of degree k can be written as

$$V(x, y) = \sum_{j=0}^{k} \alpha_j x^j y^{k-j} \tag{4.7}$$

where α is simply a coefficient. There is a theorem [11], that states: *The Hamiltonian System with the homogeneous potential V of third degree is meromorphically integrable if and only if V belongs to the Table 1.* This table is reproduced in Appendix B. A system is said to be *meromorphically integrable* if it integrable, and all of its integrals are*meromorphic functions.* A meromorphic function is defined as the ratio of two *holomorphic functions*, where a holomorphic function is a function that is continuously differentiable at any point on the complex plane. Therefore, the set of meromorphic functions contains the set of all elementary functions, and we say that if a system is not meromorphically integrable, it is not integrable at all for the purposes of this project.

By observation of the table, we can see that although an arbitrary cubic potential function of two variables has four terms ($aq_1^3 + bq_1^2q_2 + cq_1q_2^2 + dq_2^3$), the table only includes potential functions with three terms. This is because any rotation or scaling of the potential function as a whole will not change the dynamics of the system, such that after any scaling and rotation, we still have the same system we started with. After some rotation, it is always possible to eliminate one of the central terms, and then a scaling can eliminate the coefficients on one of the remaining terms. Any potential function that can be derived from some scaling and rotation from a potential in the table is implied to be in the table.

If we apply this to the Hénon-Heiles potential function, we obtain the homogeneous potential of degree 3 as

$$V_3 = x^2y - \frac{1}{3}y^3 \tag{4.8}$$

No rotation or scaling of this potential will turn this potential function into one of the functions in the table, which shows that the Hénon-Heiles potential is not integrable. However, from Hietarinta [12], a change as simple as flipping the sign on the Y^3 term can make the function integrable after a 'simple rotation', which gives the integral in Equation (4.12). We will now briefly analyse the integrable potential

$$V = \frac{1}{2}\left(x^2 + y^2\right) + x^2y + \frac{1}{3}y^3 \tag{4.9}$$

From the same Lagrangian analysis performed numerous times during this project, the equations of motion are then

$$\ddot{x} = -x - 2xy \tag{4.10}$$

$$\ddot{y} = -y - x^2 - y^2 \tag{4.11}$$

which has the integral

$$I = p_xp_y + xy + \frac{1}{3}x^3 \tag{4.12}$$

We can confirm that this is an integral by testing if it is constant throughout the motion. A short series of Mathematica commands can plot the value of the integral throughout the motion, which should be a horizontal line. It

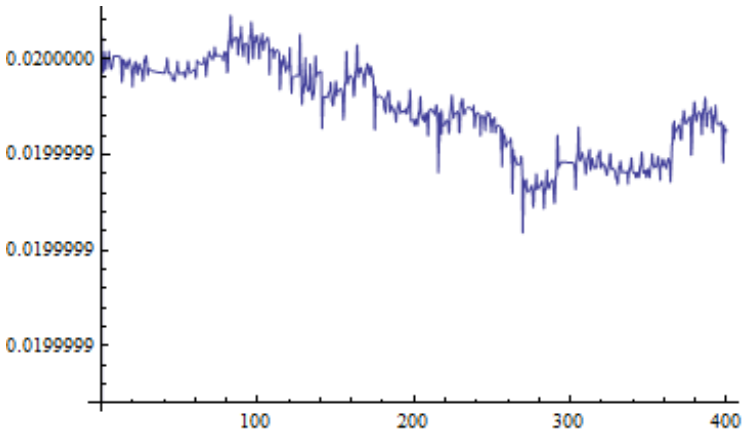

Figure 4.8: Plotting the integral over time

is worth noting that the equations of motion have been calculated through numerical integration as in Chapter 4.4 prior to this code's execution.

```
Int = D[x[t], t]*D[y[t], t] + x[t]*y[t] + x[t]^3/3 + x[t]*y[t]^2
Plot[Evaluate[Int /. sol], {t, 0, tend}]
```

The graph plotted by this code is seen in Figure (4.7). In order to interpret this graph appropriately, the scale must be observed. Although it appears spiky, the range of the graph is between 0.02 and 0.0199999. The fluctuations in the graph are merely a result of inaccuracies in the machine precision of the numerical integration, and analytically, the value remains at a constant 0.02 throughout the motion. The existence of this integral has huge impacts on the behaviour of the system as the energy level tends to the disassociation energy, as we will see in the following chapter.

Chapter 5

Chaos in Discretised Mappings

5.1 Proof of Liouville's Theorem

This chapter will analyse chaotic motion using an important technique known as plotting a Poincaré Section. Before defining what a Poincaré Section is however, it will be helpful to first prove a theorem that applies to all Hamiltonian Systems in general, and will help us to analyse the behaviour of the Poincaré Sections.

The theorem is called Liouville's Theorem, and asserts that a Hamiltonian System is *area preserving*. This means that as long as the system is Hamiltonian, if we pick a set of initial conditions, and follow how those initial conditions change over time, the area they cover will remain constant. We can prove this by making comparisons between standard phase portraits of the type seen in Chapter 2.6, and flows in fluid dynamics.

In fluid dynamics, there are two ways of analysing flow, by describing the flow in general as a vector field called the *velocity field* (Eulerian), or by tracking individual fluid particles through time (Lagrangian). For a two dimensional flow the Eulerian description takes the form

$$\dot{x}_1 = F_1(x_1, x_2, t), \qquad \dot{x}_2 = F_2(x_1, x_2, t) \tag{5.1}$$

The *streamlines* of the flow is the collection of curves that are tangent to the vector field. These can be found from

$$\frac{dx_1}{ds} = F_1, \qquad \frac{dx_2}{ds} = F_2$$

by separation of variables and integration. By equating both equations to ds, we obtain

$$\frac{dx_1}{F_1} = \frac{dx_1}{F_2}$$

For a conservative system (or *steady flow* in fluid dynamic terminology), the vector field is not dependant on time.

The alternative description, the Lagrangian description, tracks the coordinates of individual particles through time given their initial position, and is given by

$$x_1(t) = \phi_1(t, x_1^0, x_2^0), \qquad x_2(t) = \phi_2(t, x_1^0, x_2^0) \tag{5.2}$$

The velocity components can then be calculated by differentiation of Equation (5.2).

$$\dot{x}_1 = \frac{\partial \phi_1}{\partial t}, \qquad \dot{x}2 = \frac{\partial \phi_2}{\partial t} \tag{5.3}$$

Equation (5.2) is a time advance mapping of the fluid particles, because they map initial positions of the particles onto their position later on in time.

If any initial collection of fluid particles evolve under the system in such a way that their total area or volume remains constant (even if the shape of the points changes drastically) we describe the fluid as *incompressible*. In the vector field format, this can be expressed using the divergence. If the divergence of the vector field is equal to zero, by definition the fluid is incompressible.

$$\text{div}\,(\mathbf{v}) = \frac{\partial F_1}{\partial x_1} + \frac{\partial F_2}{\partial x_2} = 0 \tag{5.4}$$

For a time advance mapping, the incompressibility can be found through integration of an arbitrary initial collection of particles:

$$A_0 = \int_{D_0} dx_1^0 dx_2^0 \tag{5.5}$$

and after some time t:

$$A(t) = \int_D dx_1 dx_2 \tag{5.6}$$

where the initial domain D_0 is mapped under the effects of Equation (5.2) to D. The relationship between the two areas is given by

$$\int_D dx_1 dx_2 = A_0 = \int_{D_0} |J| dx_1^0 dx_2^0 \tag{5.7}$$

where J is the Jacobian of Equation (5.2). Under the definition of incompressibility, the areas must be the same. This is true if and only if $|J| = 1$.

It remains to link this result back to the phase flow of a Hamiltonian system. The velocity field of the Hamiltonian system can be expressed as the vector field $\mathbf{v} = (\mathbf{q}, \mathbf{p})$, where the elements of $\mathbf{v}$ are $\dot{q}$ and $\dot{p}$. For an n dimensional system, the $2n$ dimensional divergence of the velocity field is then

$$\text{div}\,(\mathbf{v}) = \sum_{i=1}^{n} \frac{\partial \dot{q}_i}{\partial q_i} + \sum_{i=1}^{n} \frac{\partial \dot{p}_i}{\partial p_i} \tag{5.8}$$

From Hamilton's Equations (2.48) and (2.49), this can be rewritten as

$$\text{div}\,(\mathbf{v}) = \sum_{i=1}^{n} \frac{\partial^2 H}{\partial q_i \partial p_i} - \sum_{i=1}^{n} \frac{\partial^2 H}{\partial q_i \partial p_i} \tag{5.9}$$

which is clearly and trivially equal to zero. This means that a Hamiltonian system behaves in the same way as an incompressible fluid from fluid mechanics, and is therefore area preserving.

5.2 Introducing Poincaré Sections

The Poincaré Section was first introduced by Henri Poincaré, a French mathematician known as 'The Last Universalist', for being the last mathematician to excel at all fields of mathematics before the subject became too advanced for one person to excel in every area [1]. The Poincaré Section requires a huge amount of numerical calculation, and while its creation was impossible in the days of Poincaré, the advancement of modern computers has made such representations possible. The code for Mathematica I have written to plot Poincaré Sections is included in Appendix A.

The Poincaré Section is a method of representing a four dimensional phase space on a lower dimensional surface. This surface S_y is the intersection of

the energy surface with $x = 0$, and typically has coordinates $(y, \dot{y})$. The surface S_x can be defined in the same way, but all Poincaré sections in this project will be plotted on the surface S_y for consistency. The position on this surface specifies the state of the system, as the two coordinates $(y, \dot{y})$ are known, as well as $x = 0$. The last coordinate $\dot{x}$ can then be solved using the Hamiltonian (but only up to a sign due to T being purely quadratic in $\dot{x}$).

As long as the trajectory is bounded, any trajectory that started on this surface will eventually cross it an infinite amount of times. If we define the initial point on S_y as $Y_0 = (y_0, \dot{y}_0)$, the trajectory will then cross back through S_y with coordinates $Y_1 = (y_1, \dot{y}_1)$. We can then define a mapping from the plane S_y onto itself, because every point $Y_0 \in S_y$ maps onto the next point $Y_1 \in S_y$. We can define the mapping symbolically as $T : Y_1 = T(Y_0)$. From Liouville's Theorem, we know that this mapping is area preserving.

5.3 Chaotic Motion and the Destruction of Tori

Before any further analysis of Poincaré Sections, it will be helpful to have one for reference. Figure (5.1) is a Poincaré Section for the Hénon-Heiles potential at energy level $H = 1/12$, tracking 10 different trajectories on the same energy level to give a wider description of the system's behaviour. The initial condition for x was set to 0, y and $\dot{x}$ were randomised, and then $\dot{y}$ was solved to keep the energy level constant.

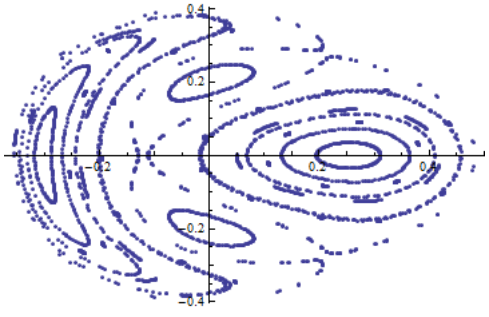

Figure 5.1: Poincaré Section of the Hénon-Heiles Potential at low energy levels

We can clearly see fixed points of centre type as seen in Chapter 2.6. These centres are the regions of intersection between the invariant tori and the $x = 0$ plane. There are no irregularities in the Poincaré Sections at this energy level, and it is easy to see that all of the trajectories plotted lie on some torus.

At higher energy levels however, as before, the regularity of the motion begins to break down. Using a Poincaré Section we can see areas of both regular and irregular motion on the same energy surface. For Figure (5.2) the energy was raised to $H = 1/8$.

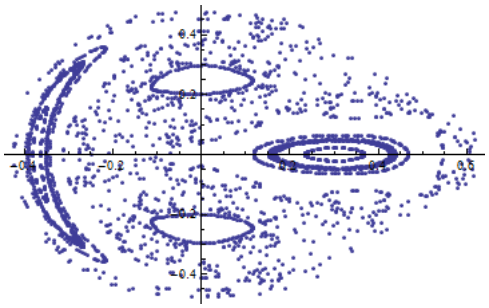

Figure 5.2: Poincaré Section of the Hénon-Heiles Potential at higher energy levels

We can see in the Poincaré Section for the raised energy surface that there are areas of both chaotic and regular motion. Some of the tori from Figure (5.1) are preserved under the higher energy level, however, some are destroyed entirely. Between the areas of regular motion, we see the trajectory wander ergodically through the section S_y on no clear pattern. The chaotic behaviour of the motion has stretched and deformed the torus such that no longer at all resembles a torus.

Figure (5.3) shows a Poincaré Section for $H = 1/6$, the disassociation energy. As we can see on this plot, the motion is almost completely chaotic, however, even up to this energy level, we see some that some tori still survive. The destruction of tori is a characteristic of non-integrable systems, such as the Hénon-Heiles potential.

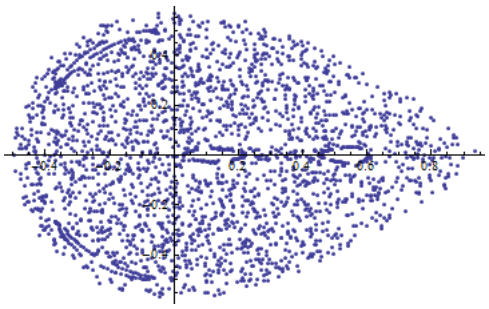

Figure 5.3: Poincaré Section of the Hénon-Heiles Potential at even higher energy levels

If we alter the coefficients of Hénon-Heiles such that it *is* integrable, as seen in Chapter 4.6, the tori are preserved up until the motion becomes unbounded. We can see this by plotting another Poincaré Section at the disassociation energy. Contour plots of this energy surface indicate that this disassociation energy is 1/12.

We can see here that when the Poincaré Section for the integrable system is plotted, there are no areas of chaotic motion at all. Every region of the section remains regular, and it is clear that the tori have remained intact. The Poincaré systems for integrable systems look much the same on all energy levels below the disassociation energy. This massive change arose from a simple change in sign in one coefficient of the potential function. This shows how close chaotic and regular systems can be to each other.

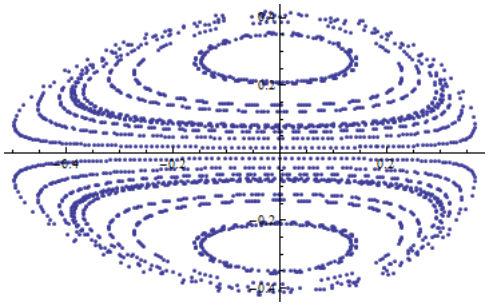

Figure 5.4: Poincaré Section of the integrable system at the disassociation energy

5.4 The Homoclinic Tangle

We can use the Poincaré Sections' behaviour to investigate the cause of the chaotic motion. By first observing Figure (5.1) we see a hyperbolic fixed point towards the middle of S_y. At the hyperbolic point, (which we denote H), four invariant curves meet. This is the same as seen in Chapter 2.6, two of the curves are ingoing, which we call H_+. Points on these curves will arrive at H after an *infinite* number of mappings of T, or $T^s X \to H$ as $s \to \infty$ if X is on H_+. The other curves are outgoing curves, H_-, and were at H an infinite number of mappings ago. $T^{-s} X \to H$ as $s \to \infty$ if X is on H_-. A hyperbolic fixed point is shown in Figure (5.5).

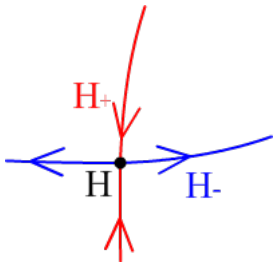

Figure 5.5: An example of a hyperbolic fixed point

The curves cannot intersect themselves, because then for a point X on the intersection of the curve with itself, the mapping would have to map X onto both curves. This cannot happen on an invariant curve. However, it is not forbidden for the curves H_+ and H_- to intersect each other (Figure 5.6). This can happen because at each point on the S_y section, the sign of $\dot{x}$is unspecified, and at the intersection, both points will have opposite signs.

This crossing of H_+ and H_- is called a *homoclinic point*. This leads to an extremely complicated property called the *homoclinic tangle*, which I will attempt to draw step by step. What remains to be seen is how the curves behave *beyond* X. To do this, we examine the effects on the mappings of the neighbourhood of X. Under iterations of T, these neighbourhoods should resemble each other, so there must be a second homoclinic point in the neighbourhood of $T(X)$ (Figure 5.7).

The area of the region R enclosed by the two curves will be important to this analysis. The same logic we used to deduce the existence of a second homoclinic point can be used to infer the existence of a third such point, another intersection of H_+ and H_- (Figure 5.8).

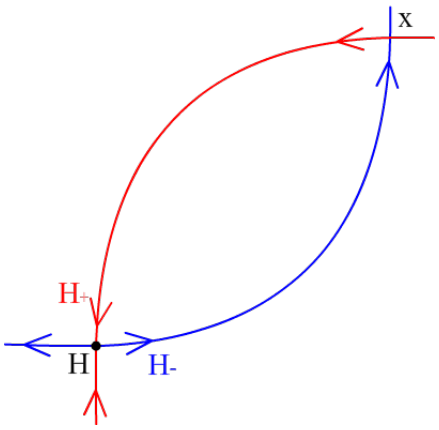

Figure 5.6: The curves H_+ and H_- intersecting at the homoclinic point X

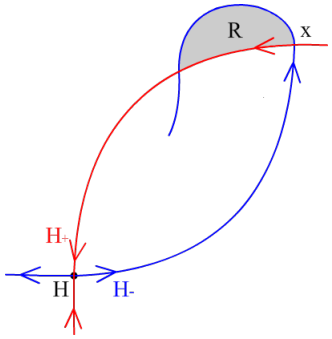

Figure 5.7: A second homoclinic point

The region of R is mapped to R' under iterations of T. The area preserving property of the Poincaré Sections implies that R and R' have the same area. The existence of a third homoclinic point implies a fourth... in general, the existence of one homoclinic point implies the existence of an infinity of others, with each additional one creating another region with the same area as R. However, there is only a finite amount of space between the homoclinic point and the hyperbolic fixed point for the curves to meet, and after more and more iterations, the homoclinic points will become closer together. To maintain the area preserving property, these loops must get longer as they get narrower. On the 'outside' of the tangle, this is easy to draw, however, the curve H_+ can not intersect itself, but must extend in an infinitely long, narrow loop. This results in each loop becoming successively

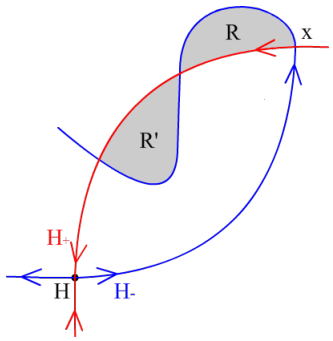

Figure 5.8: A third homoclinic point

more complicated as it winds around the homoclinic tangle (Figure 5.9).

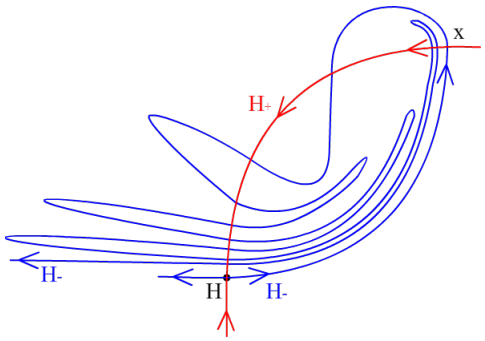

Figure 5.9: The formation of an infinity of homoclinic points

As shown in Figure (5.9), the homoclinic tangle rapidly becomes extremely complicated due to the infinitely many intersections and area preserving loops. However, this is only half the story. The same thing happens to the other curve that makes up the homoclinic tangle, and we obtain the final picture (but not a complete picture, due to only having finite amounts of time and space).

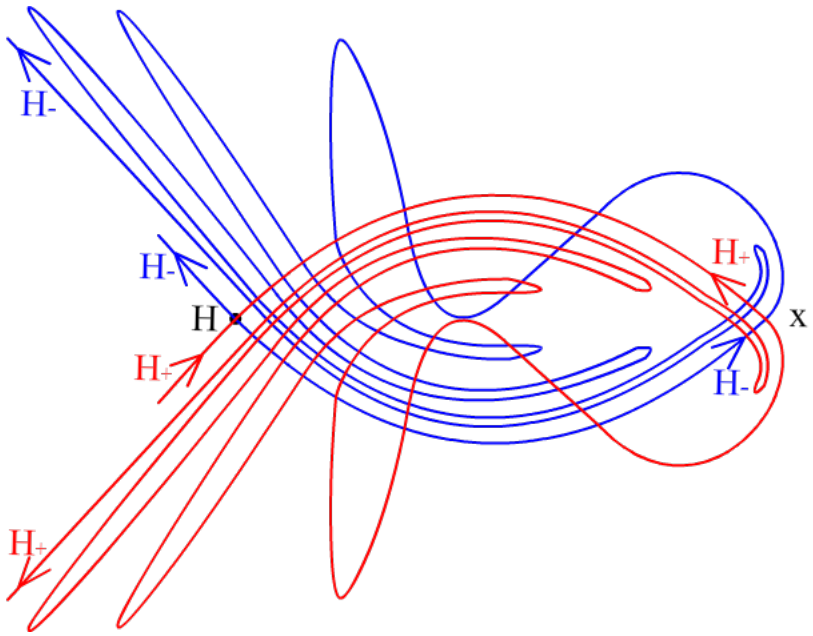

Figure 5.10: The homoclinic tangle

5.5 The Cat Map

Arnold's *cat map* is another example of a simple discrete mapping that can result in chaotic behaviour. We can define the cat map as a transformation $T\begin{pmatrix} x_n \\ y_n \end{pmatrix}$ of the 2-torus onto itself described by a transformation matrix as follows:

$$\begin{pmatrix} x_{n+1} \\ y_{n+1} \end{pmatrix} = \begin{pmatrix} 1 & 1 \\ 1 & 2 \end{pmatrix} \begin{pmatrix} x_n \\ y_n \end{pmatrix} \tag{5.10}$$

A visual description of this transformation is given in Figure (5.11).

From the transformation matrix we can obtain some properties of the mapping. Firstly, the determinant of the matrix is equal to 1, making the cat map an area preserving mapping in the same sense as the Poincaré mappings. The eigenvalues of the matrix are $\lambda_{\pm} = \frac{1}{2}\left(3 \pm \sqrt{5}\right)$, which are opposite signs. For a transformation matrix, a positive eigenvalue represents stretching in the corresponding eigendirection, and a negative eigenvalue represents shrinking.

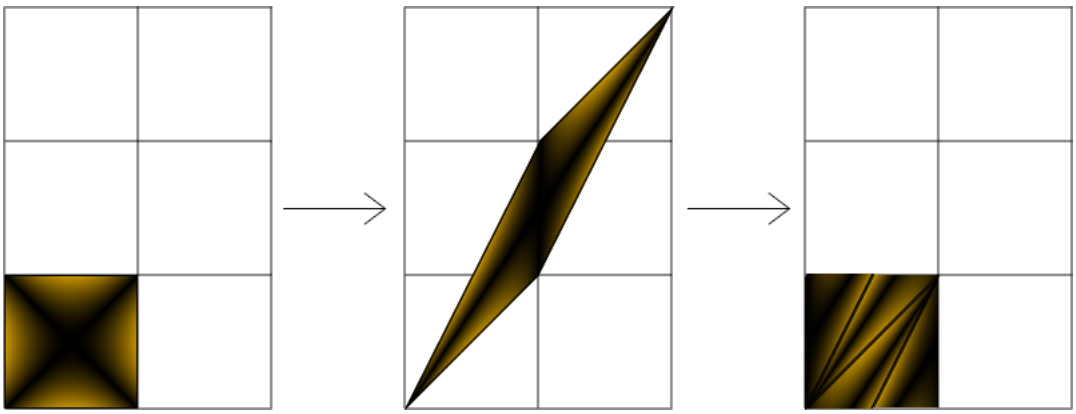

Figure 5.11: An image describing the cat map transformation

Stretching in one direction and shrinking in another indicates that all fixed points of this transformation will be of hyperbolic type.

As the mapping is defined as being on the torus, it will wrap around itself, as seen in the last image of Figure (5.10). Due to the stretching property, any small area of the image will eventually wrap densely around the torus (eventually being defined as T^{∞}). This means that any points initially close together on the image would become very far apart, and some points that were initially far apart would become close together. This sensitivity to initial conditions is an example of chaos in a discrete dynamical system. Because one point in the cat map can in theory cover the entire range of the mapping, the cat map has the ergodic property, similar to the chaotic motion from the Hénon-Heiles Potential.

However, the cat map has a stronger property than ergodicity, it is also *mixing*. This means that after T^{∞} iterations the neighbourhood of any initial point will have stretched out to cover the entire region. We can visually see the stretching and twisting of the cat map by writing a program to perform the necessary transformations to an image.

MATLAB was chosen for this task over Mathematica, and the code is given in Appendix C. The mapping has produced a mix of expected and completely unexpected results. After the first few mappings of the cat, we get the results we'd expect, the shear stretches the cat into an increasing number of narrowing strips, in which points (pixels) that started close together are pulled apart from each other. After only five iterations, the cat

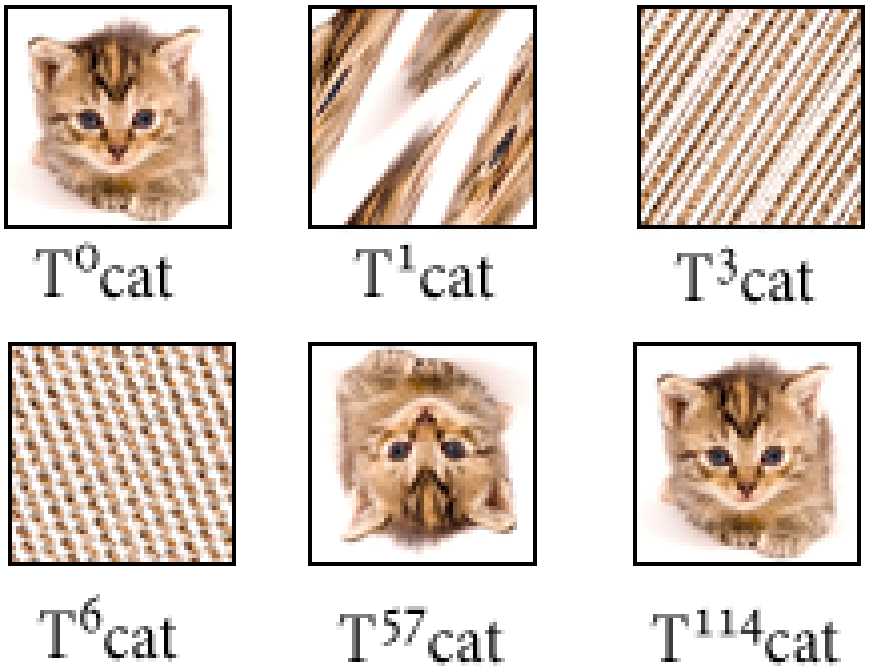

Figure 5.12: The cat at various stages of its life

has been pulled and stretched into so many pieces it is no longer recognisable. The cat has been destroyed, and we are left with a mess of random pixels representative of chaos. At this point I implore the reader not to apply this mapping to their own cat.

However, after many iterations, something completely unexpected happens, as T^{57} cat is a perfect upside-down clone of T^0 cat! If we go on a further 57 iterations of T we reverse the image again, getting T^{114} cat as an upside down version of T^{57} cat, which is of course T^0 cat. This essentially makes the mapping chaotic, yet periodic, as $\forall n \in \mathbb{N}\ T^{n+114} = T^n$.

However, this can be misleading, as the number 114 is nothing special about the mapping itself, it's a result of the initial image dimensions (74 x 74 pixels). A 150 x 150 image will take 300 iterations to return to its original form [13]. The periodicity of the cat map is simply a result of the image being represented with a finite number of pixels in a computer image file. For the 74 x 74 sized image, the most simple way to visualise this is to

imagine that every 114 iterations of T, each pixel is being moved by some number a in the x direction and b in the y direction. Due to the image being mapped on the torus, if $a = b = 0 \mod 74$, the image will have returned to its original state. For a perfectly accurate representation of this mapping with an infinite number of pixels, it would take an infinite amount of iterations to show the periodic behaviour seen above.

Chapter 6

Conclusions

In this project we have seen chaotic motion in a variety of different origins in both the continuous trajectories of the Hénon-Heiles Potential and the discretised mappings of Poincaré Sections and the Cat Map. For all systems covered in the project, visualisation has been an important part of the analysis, and a wide range of techniques were used, from manually 3D modelling the moving pendulum to writing MATLAB scripts for the Cat Map.

The visualisation, especially the Mathematica scripts on the Hénon-Heiles Potential, have clearly shown chaotic behaviour in systems that are analytically quite simple. I feel that the transition from regular to chaotic motion was shown well in the increasing levels of the Hénon-Heiles analysis, and we also saw convincing evidence from the Poincaré Sections that if a system is integrable, it does not allow chaotic motion.

While programming and visualisation has been a strong point however, there are some areas that could be improved, with more time and experience to spend on the project, like a more a mathematically rigorous classification of chaotic and regular motion using the fractal dimension of a chaotic manifold. Had I chosen to analyse the Cat Map earlier in the project, I would have devoted an entire chapter to it, and written a more detailed analysis of why the image repeats itself, and how long it takes to do so. Non-square images are also an area that could be examined in future work.

There are also many more topological aspects of chaos that would have fit in well in chapter 5, where the Homoclinic Tangle and the Cat Map were chosen for analysis. Smale's Horseshoe Map (which has many links with the

Homoclinic Tangle), and the Twist Mapping would be appropriate areas for further work. It can be shown that areas of the Homoclinic Tangle are made up of Smale's Horseshoe Maps.

Chaotic behaviour leads to a huge range of different mappings, the list of chaotic mappings is continually growing. While I could list more and more chaotic systems like the Lorenz Equations, the Logistic Map, and the Hénon Map, I feel it's best to conclude by saying that whilst there iare many more that I *could* have written, adding many more areas of content wouldn't have been appropriate, given the size of the dissertation as it is and time constraints. However, in future work, the dissertation could be referenced, and the first three chapters could be severely cut down, leaving more space and time for chaotic maps.

Appendix A

Plotting of Poincaré Sections

The following Mathematica code was used to plot all Poincaré Sections in this dissertation. The specific example below is the plot for the Hénon and Heiles system with energy 1/6.

```
eqn1 = D[x[t], t, t] + x[t] + 2 x[t] y[t];
eqn2 = D[y[t], t, t] + y[t] + x[t]^2 - y[t]^2;
T = D[x[t], t]^2 + D[y[t], t]^2;
V = 1/2 (x[t]^2 + y[t]^2 + 2*x[t]^2*y[t] - 2/3 y[t]^3);
H = T + V;
n = 10;
list = Range[n];
For[
 i = 1;, i < (n + 1), i++,
 Clear[ini];
 ics = {0, RandomReal[{0, 0.25}], 0, RandomReal[{0, 0.25}]};
 inisol =
  Solve[1/2 (0^2 + 2 0^2* ics[[2]] + ics[[2]]^2 - (2*ics[[2]]^3)/3) +
     1/2 (ini^2 + ics[[4]]^2) == 1/6, ini];
 inival = ini /. inisol;
 ics = {0, ics[[2]], inival[[2]], ics[[4]]};
 tend = 900;
 Section =
  Reap[NDSolve[{eqn1 == 0, eqn2 == 0, x[0] == ics[[1]],
     y[0] == ics[[2]], x'[0] == ics[[3]], y'[0] == ics[[4]]}, {x,
```

```
     y}, {t, 0, tend}, MaxSteps -> 100000,
    Method -> {"EventLocator", "Event" -> x[t],
      "EventAction" :> Sow[{y[t], y'[t]}]}]];
 Section2 = Delete[Section, 1];
 Section3 = Section2[[1]];
 Section4 = Section3[[1]];
 list[[i]] = ListPlot[Section4]]
Show[list, PlotRange -> All]
```

Appendix B

Meromorphically Integrable Potentials

Table 1, from [11], where a and c are arbitrary constants.

Case	Potential
(3)1	q_1^3
(3)2	$q_1^3/3 + cq_2^3/3$
(3)2'	$aq_1^3/3 + q_1^2q_2 + q_2^2/6$
(3)3	$q_1^2/2 + q_2^3$
(3)3'	$\pm\imath 7q_1^3/15 + q_1^2q_2/2 + q_2^3/15$
(3)4	$q_1^2q_2/2 + 8q_2^3/3$
(3)4'	$\pm\imath 14\sqrt{14}q_1^3/90 + q_1^2q_2/2 + q_2^3/45$
(3)5	$\pm\imath\sqrt{3}q_1^3/18 + q_1^2q_2/2 + q_2^3$
(3)5'	$\pm\imath 3\sqrt{3}q_1^3/10 + q_1^2q_2/2 + q_2^3/45$
(3)5"	$\pm\imath 11\sqrt{3}q_1^3/45 + q_1^2q_2/2 + q_2^3/10$

Appendix C

The Cat Map

```
I = imread('cat.jpg');
for alpha=1:114
tic
s=size(I);
x=s(1)
y=s(2)

tform = maketform('affine',[1 -1 0; -1 2 0; 0 0 1]);
J = imtransform(I,tform);

sT=size(J);
xT=sT(1);
yT=sT(2);

for i=x+1:2*x
    for j=1:y
        colour=J(i,j,1)+J(i,j,2)+J(i,j,3);
        if colour~=0
            J(i-x,j,:)=J(i,j,:);
        end
    end
end

for i=(2*x)+1:xT
    for j=1:y
```

```
        colour=J(i,j,1)+J(i,j,2)+J(i,j,3);
        if colour~=0
            J(i-2*x,j,:)=J(i,j,:);
        end
    end
end


for i=1:x
    for j=y+1:yT
        colour=J(i,j,1)+J(i,j,2)+J(i,j,3);
        if colour~=0
            J(i,j-y,:)=J(i,j,:);
        end
    end
end
for i=x+1:2*x
    for j=y+1:yT
        colour=J(i,j,1)+J(i,j,2)+J(i,j,3);
        if colour~=0
            J(i-x,j-y,:)=J(i,j,:);
        end
    end
end
J=[J(1:x,1:y,:)];

alpha
imshow(I), figure, imshow(J)
I=J
end
toc
```

Appendix D

Project plan

Final Year Project Plan

Chaotic Motion Revealed by the Poincaré Section

Student: Harry Green.

Supervisor: Dr. Thomas Waters

Project Outline

This project will investigate the areas of nonlinear dynamical systems that give rise to chaotic motion. Chaotic, seemingly random motion, can arise from rather simple observable and measurable systems, described by a nonlinear deterministic equation with two degrees of freedom and a high sensitivity to initial conditions. These nonlinear equations will be formulated from physical problems from classical mechanics under which energy is conserved, and from the resulting analysis we shall see chaotic motion appear in these systems.

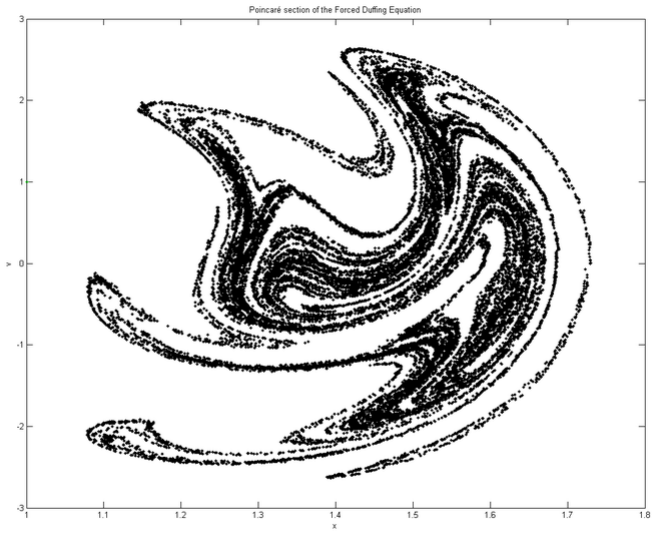

Figure D.1: The Poincaré Section will be central to detecting Chaotic Motion. This one was taken from Wikipedia

While chaos is ubiquitous in the modern sciences, and examples of chaos can be drawn from any scientific field, the project will focus on Hamiltonian systems, physical mechanical systems under which energy is conserved. A prominent example of this type of system resulting in chaos is the double pendulum, which consists of a pendulum, assumed to be smooth with no damping, and a similarly damping free pendulum hanging from it. This system, which can be defined simply in terms of two variables, can exhibit complicated dynamics despite the simple nature of the problem. Another Hamiltonian system that displays chaotic motion is the solar system, long believed to be the epitome of clockwork deterministic mechanics.

Certain *formalisms* will be introduced and defined before an in depth analysis of chaotic systems is attempted. Simple theory of stability in dynamical systems with various degrees of freedom and a well defined potential function will be introduced first, as this is the fundamental analysis which shall be developed throughout the project. This will be followed by an overview of Lagrangian Dynamics, and the formulation of the Lagrangian function $L(\mathbf{q}, \dot{\mathbf{q}}, t) = T(\mathbf{q}, \dot{\mathbf{q}}, t) - V(\mathbf{q})$, and the Lagrange form of the equation

of motion:

$$\frac{d}{dt}\left(\frac{\partial L}{\partial \dot{q}_k}\right) - \frac{\partial L}{\partial q_k} = 0$$

Generalised momenta and the Hamiltonian function will also be integral to this project, and a detailed explanation will follow the Lagrangian. The Hamiltonian is given by

$$H(q,p) = \sum_{x=1}^{n} p_x \dot{q}_x - L,$$

where n is equal to the number of the degrees of freedom of the system, and P_x are the generalised momenta

$$p_x = \frac{\partial L}{\partial \dot{q}_x}.$$

It will be shown that the Hamiltonian is equal to the total energy of the system, so that $H(\mathbf{q}, \dot{\mathbf{q}}, t) = T(\mathbf{q}, \dot{\mathbf{q}}, t) + V(\mathbf{q})$, and therefore for a system in which energy is conserved,

$$\frac{dH}{dt} = 0.$$

After establishing the Hamiltonian Formulation and Lagrangian, the final and main part of the project will be the use of a Poincaré Section to detect chaotic motion. A Poincaré Section represents a subspace of the original dynamical system with a lower dimension, preserving the properties of the system but producing a more descriptive mapping that will prove useful in showing where a system does and doesn't display chaotic behaviour. The Poincaré Section will be applied to the Hamiltonian systems described earlier, and we shall see areas of chaos in these simple deterministic systems.

This part of the project will rely heavily on many aspects of geometry and topology. Various manifolds created from trajectory paths will be used in the modelling of physical systems, such as the torus, representing regular motion, and broken tori, representing chaotic motion. Homoclinic tangles will also be important to the project due to their close links with chaotic motion.

Figure D.2: The Torus is a Manifold that will appear often in the project. This one was rendered in Autodesk 3DS Max

The project, including this plan, will be typeset using LaTeX, and the visualisation will be aided by numerous mathematical and graphics packages, including Mathematica for plotting graphs, MATLAB where numerical methods are required, and 3DS Max for general surface modelling where it is more convenient to use than a mathematics package.

Background Reading

1. Ian Stewart. *Does God Play Dice? The New Mathematics of Chaos.* Penguin Mathematics, 1997

2. James Gleick. *Chaos: Making a New Science.* Vintage, 1997

3. David Acheson. *From Calculus to Chaos.* Oxford University Press, 1997

4. Nina Hall. *New Scientist Guide to Chaos.* Penguin Science, 1992

Bibliography

[1] Ian Stewart (1997). *Does God Play Dice? The New Mathematics of Chaos.* Penguin Mathematics.

[2] Torok (1999). *Analytical Mechanics: With An Introduction To Dynamical Systems.* (pp89-125) Wiley-Interscience.

[3] Lorenz Attractor. Retrieved 13th February, 2012, from Wolfram's Mathworld Website: `http://mathworld.wolfram.com/LorenzAttractor.html`

[4] Partial Derivative. Retrieved 27th March, 2012, from Wikipedia: `http://en.wikipedia.org/wiki/Partial_derivatives`

[5] Torok (1999). *Analytical Mechanics: With An Introduction To Dynamical Systems.* (pp259-263) Wiley-Interscience.

[6] Božidar Jovanović (1992). *What are Completely Integrable Hamilton Systems.* The Teaching of Mathematics (13). (pp8-11)

[7] D.K Arrowsmith, C.M. Place (1992). *Dynamical Systems.* Chapman and Hall/CRC.

[8] D.A Wells (1967). *Lagrangian Dynamics.* McGraw Hill.

[9] M Hénon, C Heiles (1963). The Applicability of the Third Integral of Motion: Some Numerical Experiments *The Astronomical Journal, 69*(1), 73-79.

[10] M. V. Berry. Regular and Irregular Motion (pp57-91) *The Astronomical Journal, 69*(1), 73-79.

[11] Andrzej J. Maciejewski, Maria Przybylska (2004). All Meromorphically Integrable 2D Hamiltonian Systems with Homogeneous Potential of Degree 3 *Physics Letters A, 327*, 461-473.

[12] Jarmo Hietarinta (1986). Direct Methods for the Search of the Second Invariant *Physics Reports, 147*, p106.

[13] Arnold's cat map. Retrieved 27th March, 2012, from Wikipedia: `http://en.wikipedia.org/wiki/Cat_map`